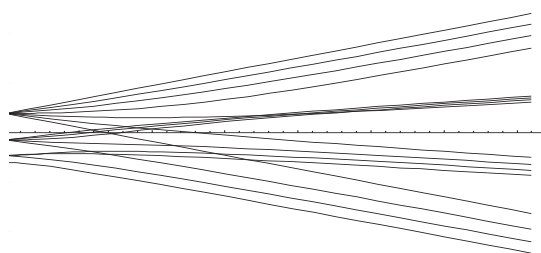


Laser System for the Stabilization of Ultracold Feshbach Molecules



MASTERARBEIT

VON

LISA KATTNER

GOTTFRIED WILHELM LEIBNIZ UNIVERSITÄT HANNOVER

FACHBEREICH PHYSIK

INSTITUT FÜR QUANTENOPTIK

Laser System for the Stabilization of Ultracold Feshbach Molecules

MASTERARBEIT

VON

LISA KATTNER

GEBOREN AM 10. OKTOBER 1982 IN BUCHHOLZ IN DER NORDHEIDE

APRIL 4, 2008

REFERENT: PROF. DR. JAN ARLT

KORREFERENT: PROF. DR. WOLFGANG ERTMER

GOTTFRIED WILHELM LEIBNIZ UNIVERSITÄT HANNOVER

FACHBEREICH PHYSIK

INSTITUT FÜR QUANTENOPTIK

Abstract

The exploration of ultracold quantum gases opens up a vast field of exciting experiments. Having achieved the first Bose-Einstein condensates and quantum degenerate Fermi gases, the mixture of those two led to the development of a new field of ultracold molecular physics. The creation of heteronuclear ground state molecules itself is a quest that demands new techniques and provides new fundamental insights in the field of molecular and many particle physics. These molecular systems offer promising possibilities in examining for example the nature of dipolar interactions.

Such heteronuclear molecules can be created by manipulating the diatomic interaction with a Feshbach resonance. These resonances occur when an atomic collision state and a quasibound molecular state coincide and can be controlled by a magnetic field. The so called Feshbach molecules are very weakly bound molecules in the highest vibrational states. Within the present experiment heteronuclear ^{40}K - ^{87}Rb molecules could be realized. One of the limiting factors in examining these molecules is their short lifetime. It was shown that it is mainly reduced due to collisions with remaining ^{87}Rb atoms. Therefore it is necessary to remove the residual ^{87}Rb atoms from the trap after the generation of molecules. To address the atoms, one has to bear in mind that the high magnetic field which is used to address the Feshbach resonance imposes a Zeeman shift on the energy transition of the ^{87}Rb atoms. A new laser system is needed that can provide these new transition frequencies.

This master thesis describes a laser system that has been realized to address ^{87}Rb atoms at high magnetic fields. The laser is stabilized to a beat signal with a reference laser. An additional microwave is used to transfer the atoms to a state at which they are resonant with the laser. The combined system uses the advantage of a highly selective microwave transition and the efficiency of atom removal through resonant laser light. This ensures a process that removes residual ^{87}Rb atoms efficiently without at the same time addressing and destroying the molecules.

Having stabilized the Feshbach molecules, the next experimental step is to optically transfer the molecules to more deeply bound vibrational levels.

Contents

1	Introduction	1
2	Ultracold quantum gases	3
2.1	History of quantum statistics	3
2.1.1	Bosonic and fermionic statistics	4
2.2	Experimental development towards ultracold quantum gases	8
2.2.1	From bosons to a BEC	8
2.2.2	Quantum degenerate fermions	9
2.3	Mixtures of ultracold quantum gases	10
3	Introduction to the K-Rb Experiment	13
3.1	Magneto-optical trap	13
3.1.1	Experimental setup of the MOT	16
3.2	Optical pumping and mechanical transfer to the science cell	20
3.3	Magnetic trap in QUIC design	21
3.4	Evaporative and sympathetic cooling	22
3.5	Magnetic transport	23
3.6	Optical dipole trap	24
3.6.1	Optical dipole force and potential	24
3.6.2	Experimental realization of the dipole trap	26
3.7	Spin preparation	26
3.8	Homogeneous magnetic field	28
3.9	Experimental improvements	30
3.9.1	Potassium laser system	30
3.9.2	Laser current controller	32
4	How to address Rb atoms at high magnetic fields	33
4.1	Interaction with an external magnetic field	34
4.1.1	Transition frequencies in the experiment	35
4.2	Blast laser system with offset lock	36

4.2.1	Laser design	37
4.2.2	Offset lock technique	40
4.2.3	Integration into the experiment	42
4.3	Microwave transition	44
5	Characterization of the blast light laser system	47
5.1	Microwave optimization	47
5.2	Laser system optimization	49
5.3	Combination of laser and microwave	50
5.4	Conclusion	53
6	Outlook	55
A	Circuit diagrams	57

Chapter 1

Introduction

A fundamental interest of humans is to find out "what holds the world together in its inmost folds" as Goethe has put it [1]. This is also what makes the research of atomic interactions as well as the creation of molecules particularly interesting. In order to look closer and closer to these phenomena, from a certain point on, one has to include quantum mechanical effects. To be able to see these effects, the object of desire has to be cooled down so that no thermal effects overshadow the quantum nature.

An often cited anecdote describes how in the beginning of the last century the young student Planck was told by his professor not to study physics because there would not be much left study. Planck did not listen to his professor, and some years later he was the first to introduce so called energy "quanta" in his famous radiation theory [2]. This was the dawn of a revolution in physics beyond comparison. The quantum world held many new discoveries and inventions, and yet led to many unanswered questions.

Current research with ultracold quantum gases tries to gain a basic insight into the quantum structure of the interactions between atoms. Of particular interest is the generation of ultracold heteronuclear molecules which will open up a field with many possible research directions.

Fundamental principles such as the search for an electric dipole moment of the electron, the parity violation and drifts of fundamental physical constants can be explored [3]. Another important research direction is the investigation of anisotropic dipolar interactions. The model for the usual scattering processes can be compared to the simple case of scattering macroscopic billiard balls. It is a very short range interaction. The anisotropic dipole interaction however has a much longer range. The quest is to achieve a dipolar gas in the ultracold quantum regime to study this interaction. First steps in this direction have been made by condensing chromium atoms and examining their dipolar behaviour in the group of Pfau [4, 5].

Compared to heteronuclear molecules, these dipole moments are relatively small and many effects may not be detectable. This makes the creation of heteronuclear molecules so interesting.

A possible application other than fundamental research was suggested by DeMille [6]. He proposed a scheme for quantum computation with ultracold dipolar molecules.

The work to which the present master thesis project contributed was started in 2004. The experiment provides a system to examine ultracold quantum degenerate mixtures of ^{87}Rb and ^{40}K , to manipulate them with Feshbach resonances and to form heteronuclear molecules of the two species. The present master thesis project's main goal was to build a laser system to enhance the lifetime of these heteronuclear molecules by removing rubidium atoms at high magnetic fields.

The thesis is structured as follows:

- The second chapter gives an overview of the historical development of ultracold quantum gases. A brief side trip to some theoretical aspects will round off the picture of quantum statistics and to conclude the overview, some major experiments that have taken place recently will be described. This will place the present experiment into the context of the latest research.
- The third chapter summarizes the experimental setup. It has already been described in previous master and PhD thesis's, therefore only the basic processes will be described. This motivates the experimental work of this master project.
- The fourth chapter describes the laser system to address ^{87}Rb atoms at high magnetic fields in detail.
- The fifth chapter presents the results of addressing atoms with the new laser system. It shows how the new system was integrated into the experiment and describes the characterization and optimization of the new laser system.
- The last chapter gives an outlook on the next steps of the experiment and future projects.

Ultracold quantum gases

2.1 History of quantum statistics

The story of ultracold quantum gases began in 1924. In this year the Indian physicist Satyendra Bose sent a paper [7] he failed to publish to his already well known colleague Albert Einstein. In this paper Bose had worked on Planck's radiation law and the statistical description of photons. Inspired by quantum mechanical principles that were still in their infancies, he considered the quantum states of photons as statistically independent instead of the particles themselves. Fascinated by this train of thought Einstein not only helped to publish Bose's paper in the renowned journal "Zeitschrift der Physik" but he also enhanced and generalized Bose's theory for ideal gases of identical atoms [8, 9].

In the course of this examination Einstein predicted that particles should theoretically condense in the lowest quantum state at very low temperatures. A first understanding of this process can be gained by considering a theory published by de Broglie not long before which states that every particle has as well wave-like characteristics. The lower the temperature, the larger is this wavelength. Decreasing the temperature and increasing the density of a gas will thus lead to average distances between the atoms so small and the de Broglie wavelength so large, that the atoms start to overlap. At this point, the so called Bose-Einstein condensation sets in.

By this time it was not known that particles can be divided into fermions and bosons depending on their spin states. Remarkably, Einstein's assumption turned out to be completely correct for bosons.

At about the same time Pauli, who was working on a completely different field of physics, the physical explanation of chemical properties of the elements, found his famous exclusion principle [10]. He used a new degree of freedom to explain the inconsistency of measured atom spectra in magnetic fields. Pauli included this

degree of freedom, which was later identified as the electron spin, to state that: "An entirely non-degenerate energy level is already closed, if it is occupied by a single electron; states in contradiction with this postulate have to be excluded". This is how he phrased his exclusion principle in his Nobel lecture [11].

Based on Pauli's discovery Fermi developed a new quantum statistical model now known as Fermi-Dirac statistics, which was in contradiction to the one Einstein had developed together with Bose [12]. In Fermi's model, a gas which is cooled down will fill up only the quantum states that are allowed by the exclusion principle even if the thermal energy would allow for lower states. At very low temperatures this results in a so called quantum degenerate Fermi sea.

It was not until 1940 and it was Pauli again, who explained the connection between the spin and if a particle follows either Bose-Einstein or Fermi-Dirac statistics, [13]. It turned out that an integer spin (bosons) means that the wave function is symmetric under exchange of indistinguishable particles and the statistics to be applied is Bose-Einstein statistics, whereas a half integer spin (fermions) indicates an antisymmetrical wave function and Fermi-Dirac statistics. For a combined particle it is the total spin that sets the rule which statistics governs its behaviour.

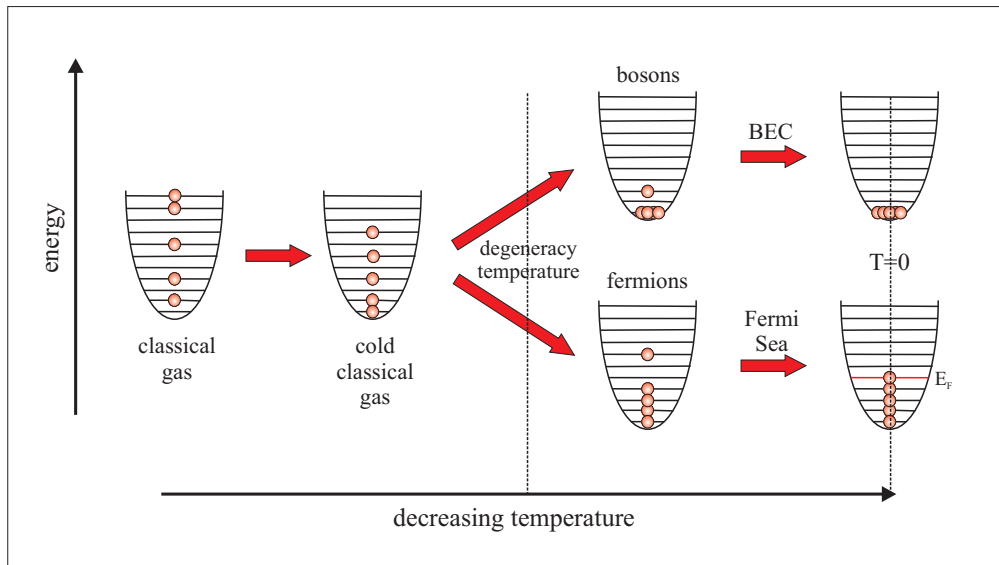


Figure 2.1: The different behavior of bosons and fermions at ultracold temperatures.

2.1.1 Bosonic and fermionic statistics

As explained above, the difference in explaining the quantum behaviour of either fermions or bosons depends on the symmetry of the wave function. To be able to describe both systems simultaneously a constant a is established:

$$a = \begin{cases} -1 & \text{Bose Einstein statistics} \\ 1 & \text{Fermi Dirac statistics} \\ 0 & \text{Maxwell Boltzmann statistics} \end{cases}$$

With this constant, the statistical behaviour can be expressed as

$$N(\epsilon_i) = \frac{1}{e^{(\epsilon_i - \mu)/k_B T} + a}. \quad (2.1)$$

This equation gives the mean occupation number N of a certain energy level ϵ_i for either bosons ($a = -1$) or fermions ($a = 1$). At high temperatures T , the constant a can be approximated with zero, which leads to the classical Maxwell Boltzmann distribution.

In this equation μ is the chemical potential. In a graphic way, it depicts the energy that is needed to add another particle to the ensemble and it is implicitly given by the normalization condition

$$\sum_{i=0}^{\infty} N(\epsilon_i) = N. \quad (2.2)$$

Bosons

The most important difference between fermions and bosons is the different behaviour at sinking temperatures. For constant particle numbers and sinking temperature, the chemical potential has to rise in order to still fulfil the normalization condition.

For bosons, the chemical potential μ is restricted by the ground state energy ϵ_0 because otherwise it would come to a physical meaningless negative occupation number of the ground state. The maximum occupation of a thermal energy level for $\mu = \epsilon_0$ is

$$N_{max}(\epsilon_i) = \frac{1}{e^{(\epsilon_i - \epsilon_0)/k_B T} - 1}. \quad (2.3)$$

Is the amount of thermal atoms less than the total number of atoms in the ensemble, the remaining atoms accumulate in the ground state and form a Bose-Einstein condensate. The number of atoms in the BEC state is therefore

$$N_{BEC} = N_{total} - N_{thermal}. \quad (2.4)$$

In the experiment the atoms are trapped in an approximately harmonic three dimensional trap which can be described with the following harmonic potential

$$V_{harm}(\mathbf{r}) = \frac{m}{2} (\omega_x^2 x^2 + \omega_y^2 y^2 + \omega_z^2 z^2). \quad (2.5)$$

Interesting is the critical temperature at which the trapped atom ensemble will start to condense. For thermal atoms above the critical temperature, the kinetic energy is much larger than the spacing between the energy levels. Therefore discrete energy levels can be approximated by the density of states and for the number of atoms the sum over the energy levels is replaced by an integral over the density of state. Neglecting the ground state energy, the density of state can be written as

$$g(\epsilon) = \frac{\epsilon^2}{2(\hbar\omega_r)^2} \quad (2.6)$$

where ω_r is the geometric mean trapping frequency $\omega_r = \sqrt[3]{\omega_x\omega_y\omega_z}$. Note that this approximation fails for a Bose-Einstein condensed ensemble where the ground state energy cannot be neglected anymore. For the number of atoms in thermally excited states follows

$$N_{therm} = \int_0^\infty g(\epsilon)N(\epsilon)d\epsilon = \int_0^\infty \frac{\epsilon^2}{2(\hbar\omega_r)^2} \frac{1}{e^{\epsilon/k_B T} - 1} d\epsilon. \quad (2.7)$$

In this equation the chemical potential μ was neglected which is possible for thermal atoms. The solution to this integral is

$$N_{therm} = \zeta(3) \left(\frac{k_B T}{\hbar\omega_r^2} \right)^3 \quad (2.8)$$

where $\zeta(3)$ is the Riemann zeta function ($\zeta(n) = \sum_{i=1}^\infty i^{-n}$) whose solution is available in table form. For the critical temperature T_C follows

$$k_B T_C = \hbar\omega_r \left(\frac{N}{\zeta(3)} \right)^{1/3} \approx 0,94\hbar\omega_r N^{1/3}. \quad (2.9)$$

With equation (2.4) the amount of condensed atoms N_{BEC} at a certain temperature T can now be estimated to

$$N_{BEC} = N_{total} \left[1 - \left(\frac{T}{T_C} \right) \right]^3. \quad (2.10)$$

Another possibility to describe the phase transition from thermal atoms to Bose-Einstein condensed atoms is to consider the phase space density ρ_{psd} . It describes the amount of particles that are located in a cube with an edge length that corresponds to the de Broglie wave length

$$\lambda_{dB} = \sqrt{\frac{2\pi\hbar^2}{mk_B T}}. \quad (2.11)$$

Together with the spatial density of the atoms n , for the phase space density follows

$$\rho_{psd} = n\lambda_{dB}^3. \quad (2.12)$$

For a classical gas, the phase space density is a measure of the typical occupation of a one particle state. If the phase space density is in the order of one, the wave packets of the atoms begin to overlap and condensation begins.

Calculating the critical temperature not for a harmonic trap but for a homogeneous density distribution leads to

$$k_B T_C = \left(\frac{n}{\zeta(3/2)} \right)^{2/3} \frac{2\pi\hbar^2}{m}. \quad (2.13)$$

Together with the de Broglie wavelength (2.11), a critical phase space density of

$$\rho_{psd} = \zeta(3/2) \approx 2,612 \quad (2.14)$$

results.

Fermions

For fermions, the chemical potential μ is not restricted by a maximum value and therefore no macroscopic occupation of a state is possible. Following the occupation equation for fermions

$$N(\epsilon_i) = \frac{1}{e^{(\epsilon_i - \mu)/k_B T} + 1}, \quad (2.15)$$

the maximum occupation of a state is one. This corresponds to the Pauli exclusion principle and is based on the fact that fermionic wave functions are anti symmetric for the exchange of two identical particles.

Analog to the description of bosons in a harmonic trapping potential and in consideration of the Fermi-Dirac statistics follows for the occupation of thermal states in an ideal Fermi gas

$$N_{therm} = \int_0^\infty g(\epsilon) N(\epsilon) d\epsilon = \int_0^\infty \frac{\epsilon^2}{2(\hbar\omega_r)^2} \frac{1}{e^{\epsilon/k_B T} + 1} d\epsilon. \quad (2.16)$$

For $T=0$, an occupation probability of all states up to an energy E_F that is defined by

$$E_F = \mu(T = 0, N) = \hbar\omega_r(6N)^{1/3} \quad (2.17)$$

is equal to one and zero for all states above. At very cold temperatures the lowest energy states will be filled up bit by bit up to the limiting Fermi energy. There is no phase transition as for bosons, but a continuous change to the quantum degenerate regime takes place and so there is no well defined critical temperature. The Fermi temperature T_F is defined by the Fermi energy

$$k_B T_F = E_F = \hbar\omega_r(6N)^{1/3}. \quad (2.18)$$

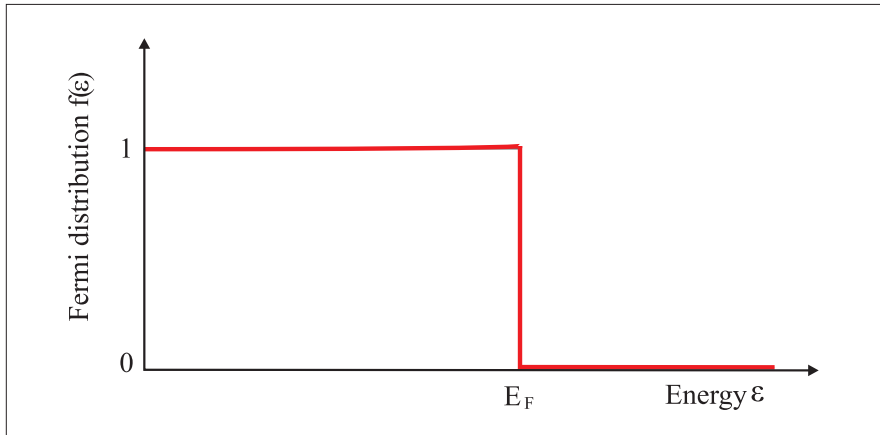


Figure 2.2: Zero temperature Fermi distribution

2.2 Experimental development towards ultracold quantum gases

2.2.1 From bosons to a BEC

Now that the theoretical part was made, the experimentalists had to draw level. Einstein himself never believed that the obscure state of condensation he predicted would ever be detected experimentally. He did not expect the enormous ambitions of the following generation of physicists.

The last century offered a vast amount of exciting discoveries to the physical world, of which some have contributed directly and some indirectly to the development of an experimental confirmation of the existence of ultracold quantum gases.

Already in 1938, experiments with cooled liquid helium led to the connection between superfluidity and Einstein's prediction of the Bose-Einstein condensation, [14], [15]. Due to the heavy interaction between helium molecules in the liquid state, no further condensation experiments were possible. It became clear that only a dilute atomic gas would lead to the expected result. Dilute gases are characterized by the fact that the density is much decreased (about a million times smaller than the density of air), so that interactions between the atoms become too small to assist the formation of a liquid and subsequent a solid at lower temperature. It is not completely avoided but delayed, comparable to supercooled water. For the achievement of quantum degeneracy, which depends on the density as well, it follows that the temperature needs to be decreased even further, to values in the regime of nanokelvin.

The development of the first laser in 1960 paved the way for the usage of radiation pressure on atoms. This process has been predicted already in 1876, as a result of Maxwell's equations. It could be confirmed experimentally in 1901 by the Russian

physicist Lebedev [16]. In 1975, the first suggestions to use the force of laser light to slow down atoms and thus cool an ensemble were made by Hänsch and Schawlow [17]. The basic principle of laser cooling is to direct a laser beam to an ensemble of atoms, so that absorbing a photon from a fixed direction and emitting it randomly leads statistically to a directed momentum transfer. Considering the Doppler shift by detuning the laser frequency and using laser beams for all spatial directions, the ensemble of atoms will be effectively cooled down. For this technique, the Nobel prize was awarded in 1997 to Steven Chu, Claude Cohen-Tannoudji and William Phillips.

Laser cooling confine the atoms in the momentum space. To trap them spatially, magnetic traps were developed, and combined with laser cooling, the first magneto optical trap (MOT) was constructed in 1987, [18]. Its temperature limit is the Doppler limit which depends on the random walk movement of scattered atoms and the shot noise of the laser light. Virtually by accident, the group of William Phillips found that for polarized laser beams in the optical molasses the atoms can be cooled down below the Doppler limit due to an effect now called polarization gradient cooling, [19], [20].

Although identified as the most promising technique, temperatures that could be reached with laser cooling in a MOT were still not low enough to reach the regime of quantum degeneracy. Another cooling technique needed to be found, and was found with the fairly simple principle of evaporation cooling. It is the same mechanism that cools a cup of coffee, by evaporating the hottest atoms from the top of a potential while the whole ensemble decreases in temperature after rethermalization, [21].

The first Bose-Einstein condensates were achieved in 1995 by the groups of Eric Cornell and Carl Wieman, [22], and Wolfgang Ketterle, [23] who were awarded the Nobel prize in 2001. Since the first BECs, lots of different and exciting experiments have developed all around the world.

2.2.2 Quantum degenerate fermions

During the thrilling race for the first BEC, the research on fermions was somewhat neglected. The experiences gained by working with ultracold bosons made fermions even more unattractive for several reasons. The most important one is the fact that the technique of evaporative cooling does not work for fermions at very low temperatures since the temperature reduction is based on the fact that after evaporation of the hottest atoms, the remaining ensemble needs to rethermalize due to collisions. For fermions at low temperatures, the Pauli exclusion principle forbids these rethermalizing collisions and the cooling effect is not present any more. Another problem is the lack of stable fermionic isotopes in alkali elements. ^{40}K is essentially stable with a half life of 10^9 years, but unfortunately it has a natural abundance of only 0,012 %.

These problems had to be overcome and 4 years after the first BEC, the group of Debbie Jin achieved the first quantum degenerate Fermi gas [24]. They developed a source of potassium that had a higher abundance of the isotope ^{40}K of 4,5 % [25] and to use the technique of evaporative cooling they prepared ^{40}K in different spin states of the hyperfine state $\frac{9}{2}$. The exclusion principle only prohibits collisions between atoms in the same spin state, while atoms with different spin state can collide and thus rethermalize.

Shortly after this first success, other groups could report on trapping and cooling ^6Li atoms to quantum degeneracy [26, 27, 28]. Instead of another spin state of the same atom, these experiments used another isotope. Bosonic ^7Li was used to rethermalize with the fermionic ^6Li during evaporation, a technique that has become known as sympathetic cooling.

Sympathetic cooling could as well be demonstrated for ^{40}K with bosonic ^{87}Rb [29]. A ^{87}Rb BEC emerging from a ^{40}K Fermi sea was achieved with this technique. It is as well the combination of elements that is used in this experiment.

2.3 Mixtures of ultracold quantum gases

Having achieved both bosonic and fermionic quantum degenerate gases, the idea of mixing those two occurs quite naturally. Several exciting effects are expected and need to be examined experimentally. The formation of ultracold molecules, consequently molecular BECs, the exploration of completely new quantum phase transitions, and heteronuclear molecules that offer promising opportunities in researching dipolar interactions, were on their way.

A powerful tool that paved the way to experimentally examine and manipulate quantum degenerate gases is the so called Feshbach resonances [30]. Feshbach resonances occur when a state of two freely colliding atoms couples resonantly with a quasibound molecular state.

In a BEC of sodium atoms these resonances were by the group of Ketterle 1998 [31]. The BEC was optically trapped in a far detuned optical dipole trap to enable a freely tuneable homogeneous magnetic field which is used to tune the Feshbach resonance. Feshbach resonances are characterized due to freely adjustable scattering properties of two colliding atoms and thus offer a completely new way of manipulating atomic interactions. The first Feshbach resonance for a fermionic quantum degenerate gas was found by the group of Jin 2002 [32].

With this new technique at hand, many exciting experiments in the quantum world can be realized. By tuning the scattering properties from repulsive to attractive, ultracold molecules can be formed. The first to realize the formation of bosonic molecules from a BEC of ^{85}Rb atoms was C. Wieman in 2002 [33]. This was followed shortly after by the creation of ultracold molecules from a Fermi gas of ^{40}K atoms by D. Jin [34]. Molecules of other fermionic species followed [35, 36]. Since fermions naturally form bosons when combined, not only ultracold molecules but

molecular BECs were created from Fermi gases [37, 35, 38].

A particular interesting and interdisciplinary research topic is the BEC-BCS crossover. It is a combination of **B**ose-**E**instein condensation and the theory of **B**ardeen, **C**ooper and **S**chrieffer, that explains solid state superconductivity by the formation of electronic Cooper pairs [39]. This theory was expanded to Cooper pairing of fermions in general. The BEC-BCS crossover appears in the vicinity of a Feshbach resonance. On the BEC side of the resonance, the scattering properties are repulsive which leads to the formation of molecules as mentioned before, whereas on the other side, the attractive properties inhibit the formation of molecules. The formation of fermionic pairs can therefore be attributed to Cooper-pairing, as in solid state superconductivity. This leads to a novel approach to understand intriguing problems of other research fields such as superconductivity and superfluidity by examining the quantum behaviour of ultracold gases. Since the first experiments in 2004 [40, 41, 42, 43], many other experiments focus on this topic.

Optical lattices have always played an important role in manipulating ultracold gases. By producing a standing light wave, a periodic potential is created in which atoms can be trapped. Optical lattices play a key role in simulating structures that can be used as precise models for solid state theory. For example are Fermions in an optical lattice a showcase analogy for an electron gas in a solid body. This has been examined extensively [44, 45, 46, 47, 48] Bose-Fermi mixtures have also been loaded into optical lattices. It could be shown that quantum degenerate fermions are transported in a one dimensional lattice due to the interaction with bosons [49]. The first heteronuclear Feshbach molecules were created in a three dimensional optical lattice in 2006 [50]. These molecules were made of ^{87}Rb and ^{40}K . Parallel to these Bose-Fermi molecules, heteronuclear Bose-Bose molecules of ^{85}Rb and ^{87}Rb were created [51].

The present experiment has been built up in the course of the research for dipole interactions to provide ultracold heteronuclear molecules of ^{87}Rb and ^{40}K in a harmonic trap.

Introduction to the K-Rb Experiment

This chapter will give an overview of the whole experimental setup that has been built up the last 4 years. Due to the complexity of the experiment and because it has already been described in detail before, see [52, 53, 54], this chapter will not focus on completeness but on the comprehensibility of the system.

The chapter is divided into parts that follow the chronological sequence of the experiment. First, the **magneto optical trap** (MOT) where the atoms are trapped and precooled is described. The vacuum cell of the MOT is spatially separated from the experimental cell where better vacuum and optical access can be realized. After preparing the atoms in the right spin state, a moveable magnetic trap transfers the atom ensemble mechanically from the MOT cell to the experimental cell. Here it is loaded into a magnetic QUIC trap, where radiofrequency evaporative cooling for the bosons and sympathetic cooling for the fermion lead to temperatures of the ensemble of about $1\mu K$. To precisely adjust the position of the atom ensemble in the trap, a technique of magnetic transport has been developed. For further experiments, an optical dipole trap is used to confine the atoms. In this trap, the atoms are then cooled down to quantum degeneracy. The generation and calibration of a homogeneous magnetic field is explained, which is used for controlling Feshbach resonances. Finally, some renewals to the existing system are described that have been contributed during this master project.

3.1 Magneto-optical trap

The principle of a magneto-optical trap bases on the technique of laser cooling paired with the spatial confinement of a magnetic trap.

Laser cooling uses the fact that photons transfer momentum on atoms. If an atom

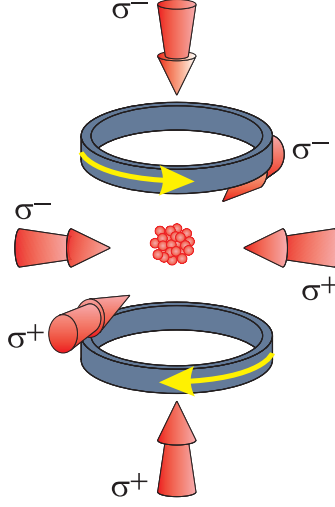


Figure 3.1: Magneto-optical trap with magnetic coils in anti Helmholtz configuration and six laser beams.

absorbs photons from a certain fixed direction while the emission is randomly distributed over all directions, the average momentum transfer will impose a directed force onto the atom. The resulting force of two directed beams in opposite directions is

$$\mathbf{F}_{\pm} = \pm \frac{\hbar \mathbf{k} \Gamma}{2} \frac{I/I_0}{1 + I/I_0 + (2(\delta_L \mp |\mathbf{k}\mathbf{v}|)/\Gamma)^2} \quad (3.1)$$

for each beam respectively. It depends on the decay rate Γ , the ratio between laser intensity and saturation intensity I/I_0 , the detuning of the laser compared to the resonance frequency $\delta_L = \omega - \omega_0$ and the Doppler shift $|\mathbf{k}\mathbf{v}|$ that includes the motion of the atoms with velocity \mathbf{v} and direction \mathbf{k} .

The total force that is imposed on the atoms is

$$\begin{aligned} \mathbf{F}_{tot} &= \mathbf{F}_+ + \mathbf{F}_- \\ &= \frac{\hbar \mathbf{k} \Gamma}{2} \left[\frac{I/I_0}{1 + I/I_0 + (2\delta_+/\Gamma)^2} - \frac{I/I_0}{1 + I/I_0 + (2\delta_-/\Gamma)^2} \right]. \end{aligned} \quad (3.2)$$

In this equation the complete detuning is $\delta_{\pm} = \delta_L \mp |\mathbf{k}\mathbf{v}|$. The velocity and detuning dependence of the force leads to an acceleration of the atoms for blue detuning of the laser frequency ($\delta_L > 0$), while for red detuning ($\delta_L < 0$) the force acts against the direction of the atom velocity and results in a deceleration of the atoms. This decelerating force is only effective for low atom velocities as indicated in figure 3.2.

By shining six red detuned laser beams onto an ensemble of atoms and thus covering each spatial direction, the atoms are effectively slowed down and the ensemble is cooled. This temperature is limited to the fact that the momentum transfer from a photon to an atom can only statistically be considered directed. This means that for each single photon that is absorbed or emitted, the atom

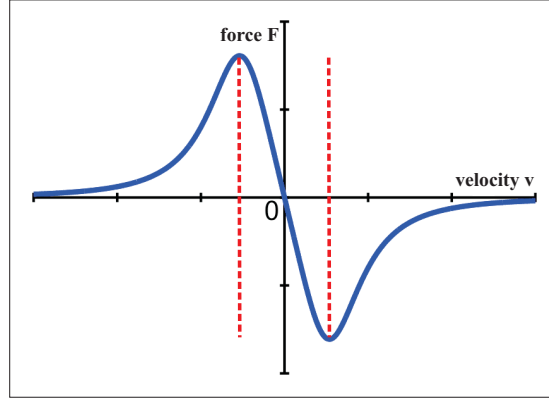


Figure 3.2: Illustration of the velocity dependence of the force, for a red detuned laser. In the marked velocity region the force acts as a linear braking force: $\mathbf{F} = -\alpha\mathbf{v}$.

obtains a random momentum and performs a random walk motion. The resulting Doppler temperature T_{dop} limits the cooling process.

$$T_{dop} = \frac{\hbar\Gamma}{2k_B}. \quad (3.3)$$

It is proportional to the decay rate Γ of the excited energy level.

By adding a magnetic field to the laser cooled atoms, it is possible to confine the cooled atoms to the middle of the trap. The Zeeman effect will split the energy levels to their magnetic sublevels m_F depending on the strength of the magnetic field

$$E = m_F g_F \mu_B B \quad (3.4)$$

with μ_B the Bohr magneton, g_F the gyromagnetic factor, m_F the magnetic sub-level quantum number, and B the external magnetic field. The Zeeman effect is explained in more detail in section 4.1.

This leads to the effect that the resonance of the transition with the laser frequency is shifted as well. By realizing a linear inhomogeneous magnetic field that is zero in the middle of the trap, the atoms will be resonant to the laser depending on their position. Splitting into magnetic sublevels results also in a polarization dependence of the transition. To address a transition that has a positive change of the m_J quantum number ($\Delta m_J = +1$), right circular polarized light is needed, respectively with a negative change ($\Delta m_J = -1$) and left circular polarized light. Linear polarized light can only address transitions that have the same m_J quantum number ($\Delta m_J = 0$).

To address the highest energetic quantum level of an atom in the negative magnetic field region, the laser beam has to be polarized right circular and in the positive magnetic field region respectively left circular. The force that is applied to the atom is the same as in equation 3.1 except for an additional detuning term δ_B due to the frequency shift of the magnetic field.

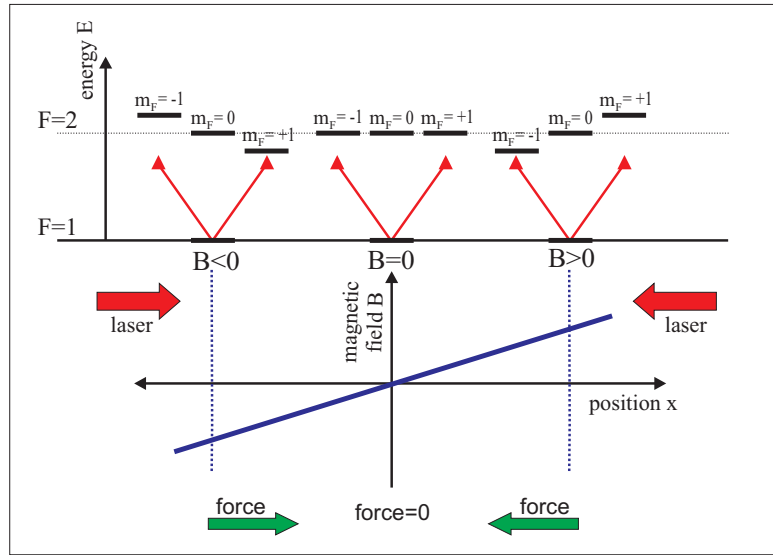


Figure 3.3: Schematic illustration of the energy level shift for an applied magnetic field B . Left circular polarized light drives a transition with $\Delta m = -1$ and right circular polarized light drives a transition with $\Delta m = +1$. The direction of the resulting force is indicated.

3.1.1 Experimental setup of the MOT

The experiment is located on two tables, one containing the lasers and necessary optical components ("optics table") and one for the vacuum chamber ("vacuum table"). The laser light is delivered to the vacuum chamber by optical fibers. This has the advantage of an easier readjustment on each side in case of changes of the experimental apparatus.

Laser system

For cooling and trapping ^{87}Rb two laser frequencies are needed, one to address the cooling transition $|F = 2\rangle \leftrightarrow |F' = 3\rangle$, and one to repump atoms from the $|F = 1\rangle$ state to $|F' = 2\rangle$. Figure 3.4 shows the Hyperfine structure of ^{87}Rb in the $5^2S_{1/2}$ ground state and in the $5^2P_{3/2}$ excited state. The arrows indicate the cooling and the repumping transition which are used for operating the MOT.

The ^{40}K transition for cooling and repumping, as depicted in figure 3.5, are only 1285 MHz apart, a distance that can be overcome with **acousto optic modulators** (AOM). Therefore only one laser is needed. The laser system for potassium is described extensively in [54]. The laser itself was recently replaced and the new design will be described more detailed in section 3.9.1.

The lasers in use for the magneto-optical trap are diode lasers with external cavities (ECDL) stabilized to a Doppler free saturation spectroscopy signal. With

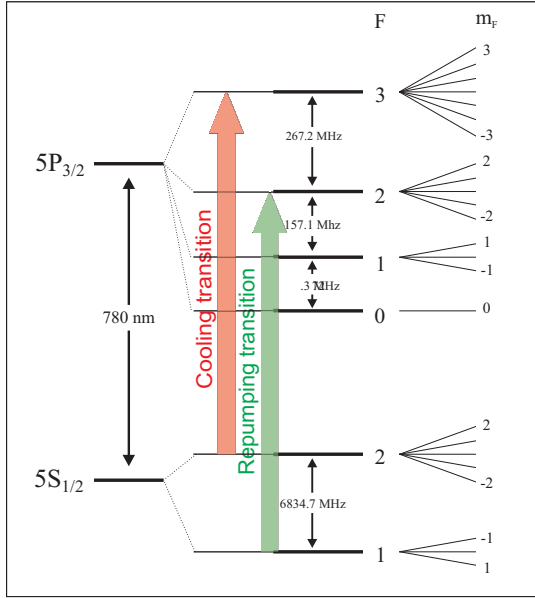


Figure 3.4: ^{87}Rb fine and hyperfine structure with indicated laser transitions

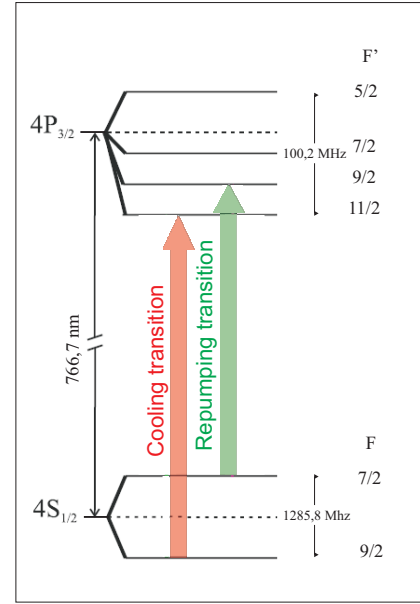


Figure 3.5: ^{40}K fine and hyperfine structure with indicated laser transitions

AOMs the lasers can be operated fast and freely adjusted to different frequencies. Table 3.1.1 shows the different transitions, the detuning and the laser output power with which the experiment is operated. To ensure a suitable small laser linewidth,

^{87}Rb	transition $5^2S_{1/2} \rightarrow 5^2P_{3/2}$	det. [MHz]	power [mW]
cooling laser	$F = 2 \rightarrow F' = 3$	-26	360
repumping laser	$F = 1 \rightarrow F' = 2$	0	20
detection	$F = 2 \rightarrow F' = 3$	0	0,5
molasses	$F = 2 \rightarrow F' = 3$	-80	250
opt. pumping	$F = 2 \rightarrow F' = 3$	+10	0,5
^{40}K	transition $4^2S_{1/2} \rightarrow 4^2P_{3/2}$	det [MHz]	power [mW]
cooling laser	$F = 9/2 \rightarrow F' = 11/2$	-34	360
repumping laser	$F = 7/2 \rightarrow F' = 9/2$	0	90
detection	$F = 9/2 \rightarrow F' = 11/2$	0	0,7
molasses	$F = 9/2 \rightarrow F' = 11/2$	-18	360
opt. pumping	$F = 9/2 \rightarrow F' = 9/2$	+32	0,3

Table 3.1: Overview of the laser frequencies and output power for operating the experiment with ^{87}Rb and ^{40}K .

new current controllers [55] were installed in the course of this master thesis. They

are described in section 3.9.2.

Figure 3.6 depicts the schematic set up of the optics table. The cooling laser serves four different purposes, the first of course is to address the cooling transition for the MOT, the second is to provide light for optical pumping, the third is to detect ^{87}Rb atoms in the $|F=2\rangle$ state and the last is to provide light for a beat signal with the high detection laser which will be described detailed in chapter 4. It is superimposed with the repumping laser to inject a tapered amplifier (TA) to increase the output power. For the detection of the $^{87}\text{Rb}|F=1\rangle$ state, a small amount of light is branched off the repumping laser.

The ^{40}K laser is preamplified with a TA, and to clean spatial mode it is guided through a single mode fiber. Then it is divided into cooling and repumping light. Both beams are amplified again with another TA and then superimposed with the cooling and repumping beams for ^{87}Rb on to a fiber that guides the light to the MOT. For ^{40}K detection and optical pumping, light of the ^{40}K cooling laser is branched off and superimposed with ^{87}Rb light of the same purpose.

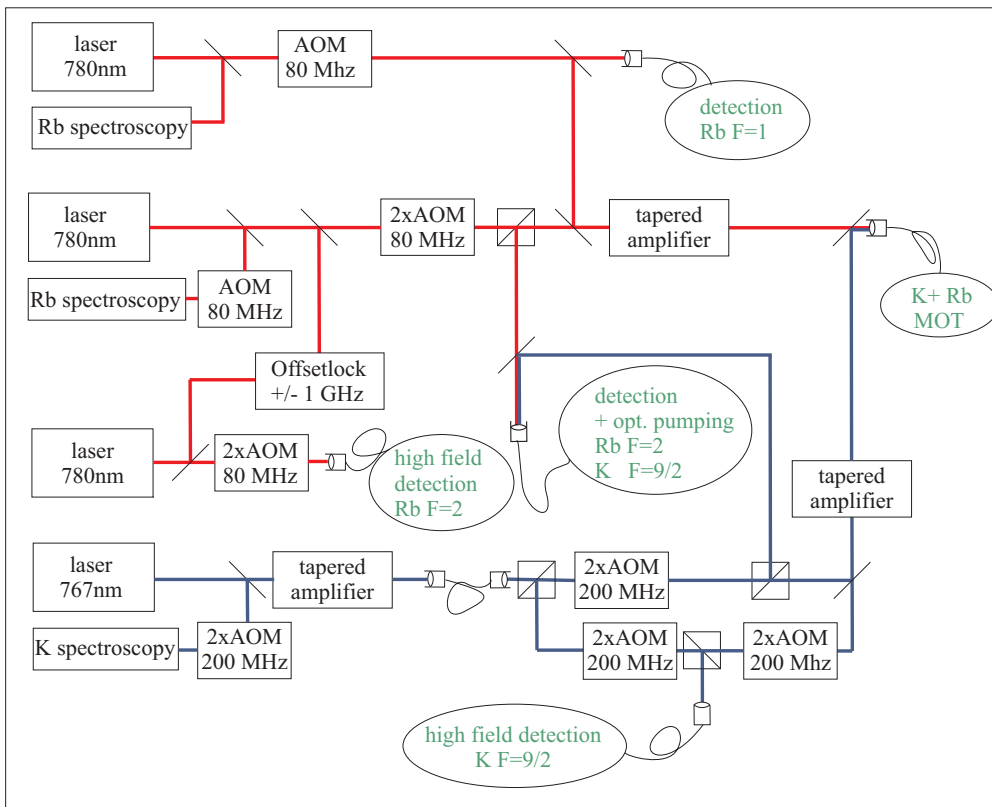


Figure 3.6: Schematic illustration of the lasersystem.

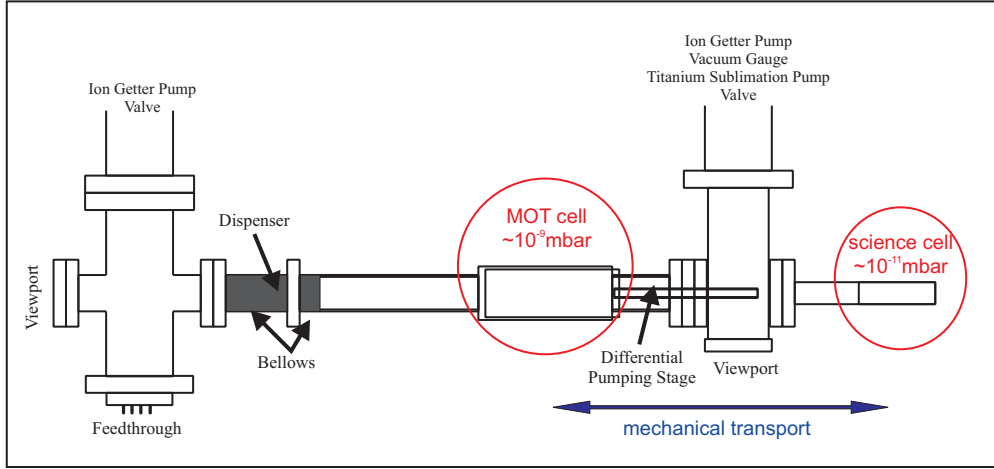


Figure 3.7: Schematic illustration of the vacuum system [53].

Vacuum system

The vacuum chamber is divided into two parts, one for the MOT where a vacuum of $\sim 10^{-9}$ mbar can be achieved, and a second where the actual experiments take place at a vacuum of $\sim 10^{-11}$ mbar, called "science cell". These two parts are separated by a differential pumping stage. This division has the advantage that while the MOT is loaded from background gas of ^{40}K and ^{87}Rb atoms in the MOT cell at a higher pressure, the scattering effects with background gas are highly reduced in the science cell and provide the appropriate conditions to cool down the atoms. This design also provides optimal optical access to the science cell. Two ion getter pumps at each cell provide the needed pumping power to sustain the vacuum.

The atomic background gas is released by dispensers [25] that are located in the MOT region. It is sufficient to heat the dispensers about once a week by passing a current through them. In addition a technique to quickly raise the background gas pressure to load the MOT, called light induced atom desorption (LIAD) technique is employed. Ultraviolet light is used to desorb atoms which are attached to the cell walls. This strongly increases the background gas pressure for the time the UV light is switched on. The method is described in detail in [56].

In the MOT, atom numbers of $8 \cdot 10^9$ for ^{87}Rb and $1 \cdot 10^8$ for ^{40}K are achieved.

Cooling below the Doppler limit

To cool down the atoms below the Doppler limit, a technique has been developed that is called polarization gradient cooling. It is based on spatial variable light fields induced by superimposed laser beams that generate a shift of the atomic energy levels. This shift can be described in the dressed atom picture [20].

There are different approaches to realize polarization gradient cooling. The one used in this experiment has an arrangement of two counter propagating laser beams with left and right circular polarization respectively. This results into a linear polarized light field whose polarization rotates around the axis of the \vec{k} vector. Descriptively described, this arrangement creates different occupation probabilities for the ground state level depending on the motion direction of the atoms. This results in different absorption probabilities for left and right circular polarized light. Averaged over time, the atoms absorb counterpropagating photons more often and thus, are slowed down.

The temperature that can be reached is again limited, this time by the recoil energy of a single spontaneous emission process

$$E_{rec} = \frac{(\hbar k)^2}{2m}. \quad (3.5)$$

With this energy, the so called recoil limit temperature is

$$T_{rec} = \frac{E_{rec}}{k_B} = \frac{(\hbar k)^2}{2mk_B}. \quad (3.6)$$

It is the last spontaneous emission of a cooling process that leaves the momentum $\hbar k$ to the atom.

To cool down the atoms down to the recoil limit in the experiment, a period with a pure optical molasses without magnetic trap follows the MOT period. The MOT light is used to produce the red detuned, contrary circular polarized laser beams in opposite directions that are needed for polarization gradient cooling.

3.2 Optical pumping and mechanical transfer to the science cell

In a magnetic quadrupole trap only so called low field seeking atoms can be trapped. These atoms have a positive product of their gyromagnetic factor and magnetic sublevel number and therefore they are attracted to the lowest magnetic field in the middle of the trap. During the MOT phase the atoms are in a mixture of different spin states. Optical pumping is used to prepare the atoms in a spin polarized mixture. For ^{87}Rb the atoms are prepared in the $|F = 2, m_F = 2\rangle$ state, the ^{40}K atoms are prepared in the $|F = 9/2, m_F = 9/2\rangle$ state. For optical pumping, MOT laser beams and magnetic field are switch off, and a linear magnetic field of 1G and the pump laser light is applied.

After the optical pumping, the atoms are trapped by a quadrupole potential provided by the same coils that were used to operate the MOT. To compress the atoms spatially in the trap, the magnetic field is increased. The size of the atomic

cloud is limited due to the fact that it has to fit through the differential pumping stage in the following transport to the science cell.

The two coils that generate the quadrupole trap are mounted on a movable transport rail. This transport system transfers the coils, and hence the trapped atomic cloud from the MOT cell through the differential pumping stage to the science cell where the actual experiments take place.

3.3 Magnetic trap in QUIC design

Atoms in the middle of a quadrupole trap where $B = 0$ can change their spin states. This process is called a Majorana spin flip [57]. These atoms are lost from the trap if they are no longer in low field seeking states. This effect is insignificant for thermal clouds, since the density in the middle of the trap is too low. Therefore a quadrupole trap was used for the transport between the two cells without excessive loss of atoms. However, it does become a problem for very cold clouds of atoms, in particular during evaporative and sympathetic cooling. Therefore, a magnetic offset field in the trap center is needed.

This offset is added by another coil that expands the trap to a Quadrupole-Ioffe-configuration (QUIC) trap [58]. The setup of the quic trap is shown in figure 3.8. Adding the magnetic field of a QUIC coil to the magnetic field that is generated

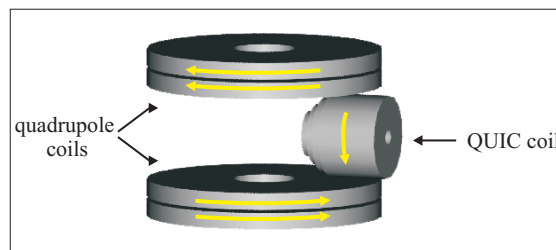


Figure 3.8: Scheme of magnetic trap in QUIC configuration. It consists of two quadrupole coils in anti Helmholtz configuration and an additional QUIC coil. The yellow arrows indicate the direction of the current flow [52].

by two quadrupole coils in anti Helmholtz configuration will lead to a deformation of the quadrupole field and a shift of its minimum. From a certain current value on, the combined magnetic field forms a harmonic potential with an offset. In case of this experiment, the current value is 25 A for all three coils and the generated offset is 1,5 G. It is an advantage of this design that the current has to be the same for all three coils. They can be connected in series which reduces the noise of the offset field and a stable offset field is important to avoid fluctuations in the trap.

3.4 Evaporative and sympathetic cooling

To decrease the temperature of the atoms in the magnetic trap, the hottest atoms are removed from the trap and after a period of rethermalization, the ensemble has a colder temperature. This is the principle of so called evaporative cooling. It is the same process that cools down a cup of coffee. The hottest atoms evaporate out of the cup and leave behind colder atoms. A main requirement for this cooling process is rethermalization, meaning the energetic equalization of the left over atoms by elastic collisions. On average all atoms will have less energy after that and the ensemble has been effectively cooled.

At low temperatures, this method only works well for the bosonic ^{87}Rb , since rethermalization collisions are forbidden for the fermionic ^{40}K . Instead, they are cooled by sympathetic cooling, which means that the colder ^{87}Rb atoms function as a cooling gas for ^{40}K . By heteronuclear collision between the two atomic species, which are not forbidden, the ^{40}K atoms adjust to the temperature of the ^{87}Rb atoms.

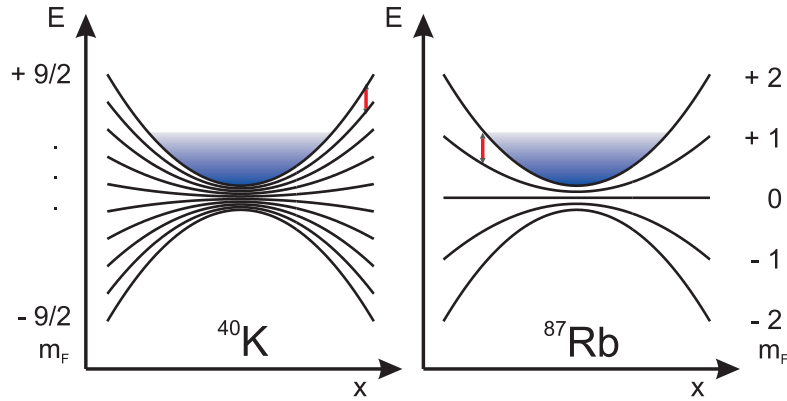


Figure 3.9: Zeeman splitting of magnetic trapped ^{40}K and ^{87}Rb . The RF frequency photon (red arrow) addresses ^{87}Rb atoms on the edge of the ensemble, and thus removes the hottest ^{87}Rb atoms evaporatively, but does not affect ^{40}K atoms [54].

To remove the hottest ^{87}Rb atoms, one can assume that they have a larger possibility of being located in the high energetic regions of the trapping potential. They perceive the highest magnetic field and thus, have the largest Zeeman splitting of their spin states. It is taken advantage of this fact by generating spin changing **radio frequency** (RF) photons that are only resonant to these hotter atoms in the outer parts of the potential. Driving the transition $|F = 2, m_F = 2\rangle \rightarrow |m_F = 1\rangle \rightarrow |m_F = 0\rangle$ will lead to a non trappable spin state and thus, the loss of ^{87}Rb atoms.

^{40}K atoms are not affected by this method because the same RF photon is not resonant to any ^{40}K transition as can be seen in figure 3.9. Therefore no ^{40}K atoms

are lost during this process.

In the experiment the number of atoms that are cooled down to quantum degeneracy at about 450 nK are $1,3 \cdot 10^6$ for ^{87}Rb and $1,3 \cdot 10^6$ for ^{40}K .

3.5 Magnetic transport

The following steps of the experiment include transferring the atoms into an optical dipole trap and then applying a homogeneous magnetic field to the atoms. Once the atoms are trapped in the dipole trap, it is convenient to use the quadrupole coils of the magnetic trap in Helmholtz configuration to generate a homogeneous field. The problem is that this field is only homogeneous in the middle of the two quadrupole coils, and as explained in section 3.3, the QUIC trap has a trapping potential minimum that is shifted compared to the middle of the quadrupole coils. The atomic ensemble trapped in the potential minimum would therefore be exposed to a magnetic gradient. To avoid this effect, the atoms are transported to the middle of the quadrupole coils. A completely new method was developed to achieve this transport and by these means, a unique method to control and manipulate ultracold quantum gases evolved [59].

In principle the transport is achieved by superimposing an extra quadrupole field on the QUIC trap that leads to a combined trapping potential whose minimum is shifted back to the middle of the original quadrupole coils.

To generate this additional field, the transport coils are used. With the transport

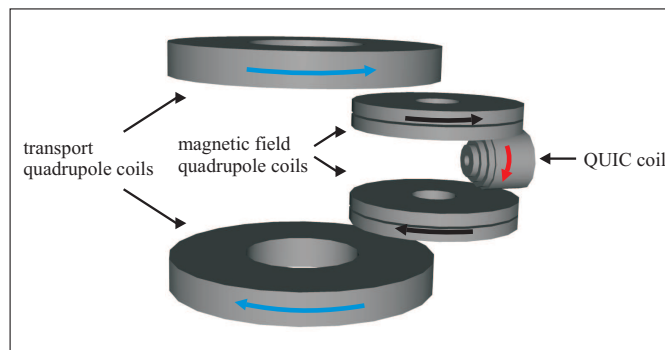


Figure 3.10: Schematic illustration of the magnetic coil configuration for the transport. The arrows mark the current that flows through the coils to generate the magnetic fields [52].

rail on which the coils are mounted, a positioning precision of $5 \mu\text{m}$ is possible. It is necessary to carefully calculate the needed currents for the five coils to avoid heating and loss of atoms. A higher offset field favors the loss-free transport because it lowers the trap frequencies and thus, density dependent loss is avoided. Figure 3.11 shows the simulated current values for the two quadrupole coil pairs

and the QUIC coil. While the current of the transfer coils is gradually increased, the current for the quadrupole coils of the magnetic trap is decreased. The graph for the QUIC coil shows the additional current that is needed to increase the offset field.

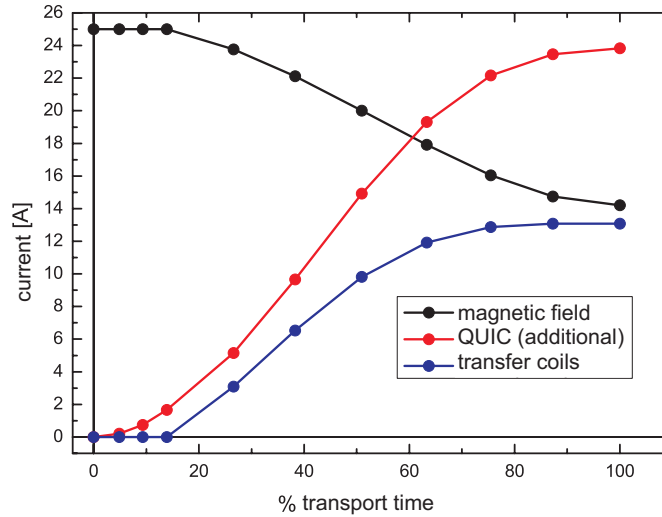


Figure 3.11: Simulation of the currents for the different coils to achieve a loss-free magnetic transport [52].

3.6 Optical dipole trap

For the following experiments, it is necessary to apply a homogeneous magnetic field to the atoms. Therefore, a magnetic trap cannot be used to confine the atoms. Instead, a dipole trap will be used. The dipole trap is based on the dipole force, which depends on the interaction of a far detuned light field with the dipole moments of the atoms. The light field is not resonant with any atomic transition and thus, does not lead to a light pressure force on the atoms as for laser cooling. Instead, in the dressed atom picture, a space dependent shift of the states is induced, and a force along the intensity gradient of the light field is produced. The optical dipole trap has been proposed in 1978 by Ashkin [60] and was realized experimentally by the group of S. Chu in 1986 [61].

3.6.1 Optical dipole force and potential

To obtain the basic idea of the optical dipole force, one can consider an atom that interacts with laser light [62]. The electric field E initiates an oscillating atomic

dipole moment with an amplitude \tilde{p} that is proportional to the amplitude of the electric field \tilde{E}

$$\tilde{p} = \alpha \tilde{E} \quad (3.7)$$

where α is the complex polarizability of the atom, depending on the driving frequency of the electric field ω . The potential is

$$U_{dip} = -\frac{1}{2} \langle pE \rangle = -\frac{1}{2\epsilon_0 c} \text{Re}(\alpha) I. \quad (3.8)$$

Thus, the potential is proportional to the intensity $I = 2\epsilon_0 c |\tilde{E}|^2$ of the electric field. Since a conservative force is the negative gradient of a potential, it is obvious that the dipole force is proportional to the gradient of the intensity

$$F_{dip} = -\nabla U_{dip} = \frac{1}{2\epsilon_0 c} \text{Re}(\alpha) \nabla I. \quad (3.9)$$

These equations are very general. To obtain a more accurate view on the dipole force, one has to examine the polarizability α in more detail.

In the semiclassical picture, one can assume the atom to be a two level quantum system that interacts with a classical electric field. Neglecting saturation effects, it can be shown that the polarizability is

$$\alpha = 6\pi\epsilon_0 c^3 \frac{\Gamma/\omega_0^2}{\omega_0^2 - \omega^2 - i(\omega^3/\omega_0^2)\Gamma} \quad (3.10)$$

where ω_0 is the resonance frequency and Γ is the damping rate that is determined by the dipole matrix element between ground and excited state.

Inserting this into formula 3.8 and using the rotating wave approximation that can be applied for detunings $\Delta = \omega - \omega_0$ that are small compared to the resonance frequency, $|\Delta| \ll \omega_0$, will lead to the following dipole potential

$$U_{dip} = \frac{3\pi c^2 \Gamma}{2\omega_0^3 \Delta} I. \quad (3.11)$$

This is the basic equation that can be used to describe the potential of far-detuned optical dipole traps. It depicts two major facts of dipole traps:

The potential scales with intensity I and detuning Δ . It means that the greater the detuning is chosen, for example to avoid resonance effects on the trapped atoms, the greater the intensity has to be to balance out the decrease in potential.

The sign of detuning indicates the type of dipole trap, either blue or red detuned. For the more common red detuned dipole trap, the detuning Δ is negative, which leads to a negative dipole potential and thus, an interaction that attracts atoms into the light field.

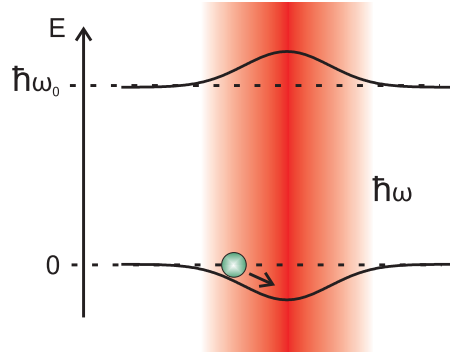


Figure 3.12: The interaction of the red detuned light field with the atomic dipole moment generates a force that is directed to the intensity gradient [54].

3.6.2 Experimental realization of the dipole trap

In the present experiment, a Nd:Yag laser (Mephisto, Innolight) at 1064 nm with a maximum output power of 2 W and a linewidth of 10 kHz is used. To obtain an approximately harmonic three dimensional trapping potential, a crossed beam dipole trap was realized.

The output of the laser is divided at a beamsplitter cube and each beam passes a 80 MHz AOM, that is used to stabilize the intensity of the beam. A small part of each beam is measured by a photo diode. This signal is used to control the power in the two AOMs. To avoid interference effects in the intersection of the two beams, a frequency difference is realized by using the 1. order after the AOM for one beam and the -1. order for the other one. To achieve a good beam profile, the two beams pass polarization maintaining fibers. The beams are focussed onto the middle of the magnetic trap by a $f = 250\text{mm}$ achromatic lens that produces a waist of $24,8\mu\text{m}$ in the horizontal direction and by a $f = 600\text{mm}$ achromatic lens and a waist of $59,5\mu\text{m}$ in the vertical direction.

By adjusting the power of the two beams, the trapping potential can be manipulated. The dipole trap is switched on while the magnetic trap is still running. High power in the beams assures a deep trap to load as many atoms as possible into the dipole trap. The magnetic trap is then switched off. Reducing the power in the two beams leads to a relaxation of the trap and a loss of the hottest atoms. This evaporation with a following phase of rethermalization cools the atoms down to almost the region of quantum degeneracy.

3.7 Spin preparation

In a dipole trap, the spin states of the atoms can be chosen freely. To examine heteronuclear Feshbach resonances, both atomic species are transferred to the lowest hyperfine states: $^{40}\text{K} |F = 9/2, m_F = -9/2\rangle$, $^{87}\text{Rb} |F = 1, m_F = 1\rangle$. This prohibits

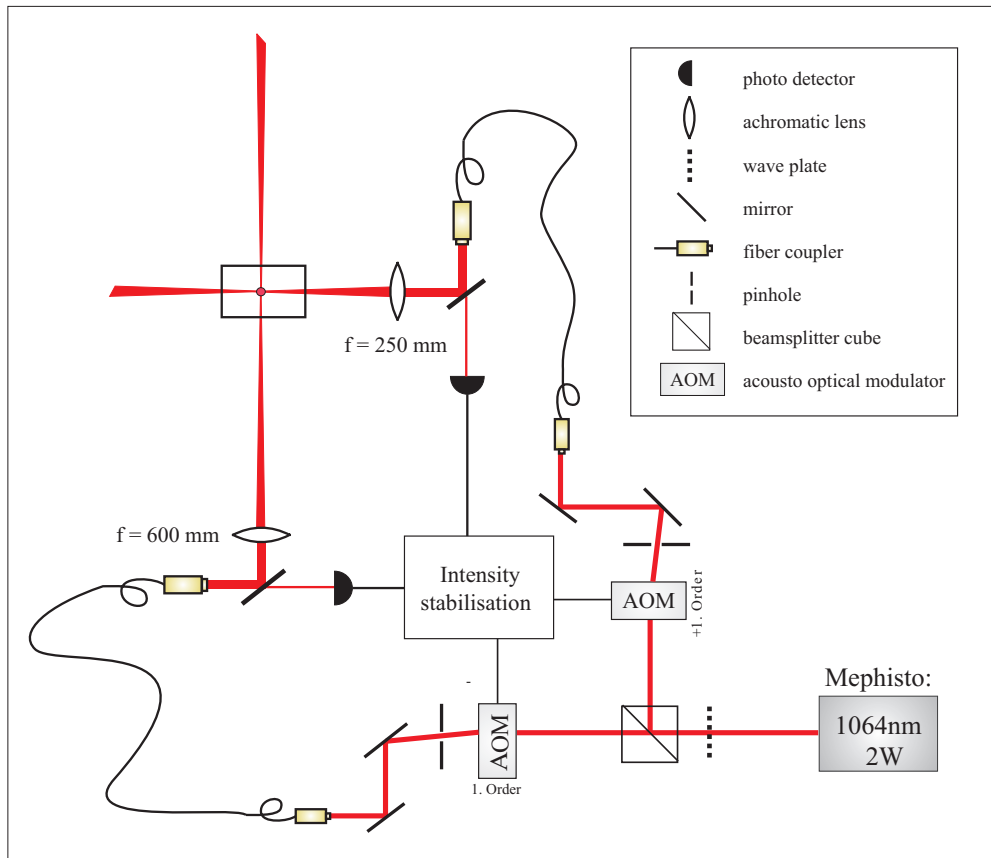


Figure 3.13: Schematic illustration of the dipole trap setup.

spin changing collisions due energy conservation. To change the hyperfine and spin states, adiabatic rapid passages are used.

The effect is based on the interaction of an atom with an electromagnetic field. The eigenstates of the system are shifted by the electromagnetic field and consist of mixtures of different magnetic sublevel states. If the field is changed adiabatically, the eigenstates follow this slow change. For resonant frequencies of the electromagnetic field, the so called diabatic states cross other atomic states. An adiabatic coupling prohibits the degeneracy of the eigenstates and so the transition to another state becomes possible. The strength of the coupling depends on the electromagnetic field intensity.

To change between the magnetic sublevel states that belong to the hyperfine state $F = 9/2$ of ^{40}K , a radio frequency ramp is used. The frequency tuning has to be fast enough compared to relaxation processes and slow enough that the state change can happen adiabatically. The frequency that is needed to transfer ^{87}Rb between two hyperfine states is much larger. For this transition, microwave radiation is used.

The left side of figure 3.14 shows the dressed atom picture of the ^{87}Rb hyperfine transition at 10 G. The energy of the coupled system $|F = 2, m_F = 2\rangle \rightarrow |F = 1, m_F = 1\rangle + \gamma$ is depicted as a function of microwave frequency. A typical frequency ramp is from 6,8561 GHz to 6,8553 GHz in about 80 ms.

The right side of figure 3.14 shows the transfer between the magnetic sublevel states of the ^{40}K hyperfine state $|F = 9/2\rangle$ at 19,6 G. The transition is addressed by a radio frequency ramp that starts at 6,56 MHz and ends between 5,79 and 6,63 MHz, depending on which state one wants to prepare.

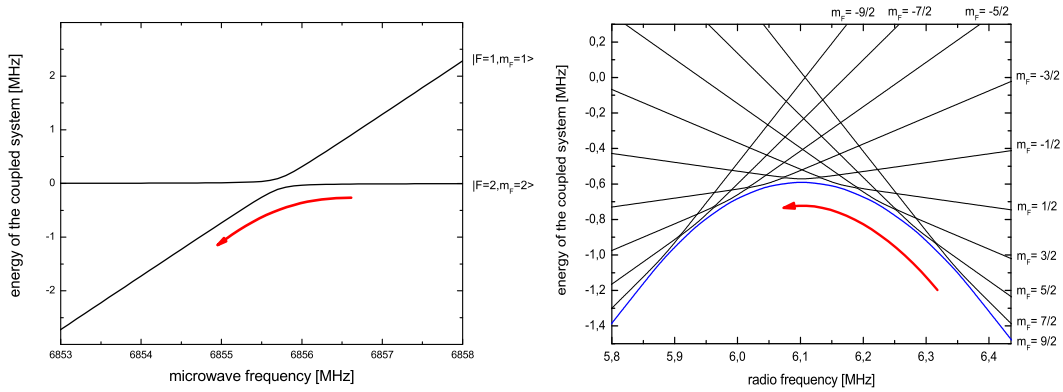


Figure 3.14: Left: adiabatic rapid passage for the ^{87}Rb hyperfine transition. Right: Adiabatic rapid passage for the ^{40}K magnetic sublevel transition [52].

3.8 Homogeneous magnetic field

For the generation of Feshbach molecules, a reliable homogeneous magnetic field is required. The two quadrupole coils of the magnetic trap are used to produce this homogeneous magnetic field. They are switched from anti Helmholtz configuration to Helmholtz configuration via a mechanical relay. The Helmholtz configuration provides an approximately homogeneous field in its center position where the atoms are located.

The Feshbach resonance that is used for the creation of molecules is located at a magnetic field of 546,7 G. With the given pair of coils this value is achieved for a current of 27,8 A. To precisely control the atomic interaction in the vicinity of the Feshbach resonance, the magnetic field has to be controllable to a certain extend depending on the size of the Feshbach resonance. For the used Feshbach resonance at 546,7 G, the magnetic field stability has to be in the range of 30 mG. To obtain this desired magnetic field stability, the current has to be stable up to 1,5 mA. The current is detected with a Hall sensor and actively stabilized with a PI controller. To decouple the control circuit from the mains current, a conventional car battery is used to operate the circuit.

The stability of the homogeneous magnetic field is measured by using an atomic microwave or radio frequency transition. This is possible with the assumption that the main contribution to linewidth of the transition is caused by the magnetic field instability. As an example, the ^{87}Rb transition $|F = 1, m_F = 1\rangle$ to $|F = 2, m_F = 2\rangle$ at a magnetic field of 546,10 is used. It is the same transition that will be used to address the ^{87}Rb atoms at a high magnetic field for the molecule stabilization, as explained in chapters 4 and 5.

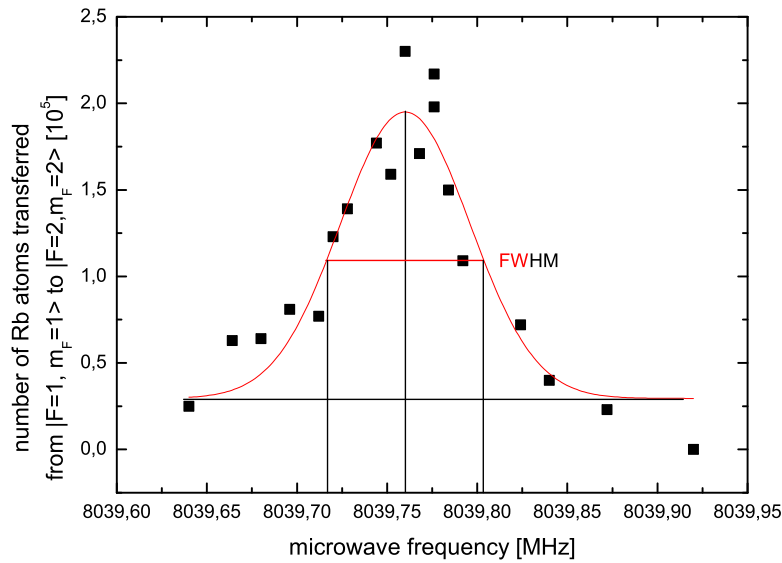


Figure 3.15: Spectroscopy of the transition $|F = 1, m_F = 1\rangle$ to $|F = 2, m_F = 2\rangle$ at a magnetic field of 546,10 G. It is fitted by a Gauss function with a FWHM of 85,07 kHz.

Figure 3.15 shows a spectroscopic signal of the transition that is obtained by scanning the microwave frequency and detecting atoms in the $|F = 2, m_F = 2\rangle$ state. At the resonance frequency, all atoms are transferred to the $|F = 2, m_F = 2\rangle$ state, whereas the larger the detuning from the resonance frequency is, the weaker is the signal of transferred atoms. The data points were fitted with a Gauss function. The full width at half maximum (FWHM) of this Gauss function is 85,07 kHz. The corresponding magnetic field width can be calculated by using the Breit-Rabi formula from section 4.1 which relates the transition frequency to a magnetic field value. This leads to a magnetic field width of 37 mG. Using this method for various magnetic fields helps to calibrate the current in the coils that generate the magnetic field.

3.9 Experimental improvements

This section emphasizes the contributions to the experiment that have been added within this master thesis project. Especially, a new potassium diode laser has been built as well as new current controllers for all the diode lasers of the experiment.

3.9.1 Potassium laser system

A new diode laser for potassium was set up. The originally used Ti:Sa had been replaced by a diode laser within the diploma project of J. Will [54]. The stability of system was improved in by replacing the formerly used diode laser with one that follows the suggested design by T. Hänsch [63].

It is a laser with an external cavity (ECDL) that enables the frequency tuning of the laser. Both the laser diode and the grating are mounted on the same temperature stabilized brass block, which is necessary for the stability of the output wavelength. To tune the wavelength to the desired value, the position of the grating can be adjusted relatively to the laser diode. This is realised by two simple cuts in the brass block on which the grating is attached, one horizontal to the grating and one vertical. They work as levers and can be adjusted with fine thread screws. A piezoelectric element that is also attached to the horizontal grating mount provides the adjustment possibilities of the cavity length by an electronic signal. Figure 3.16 shows the schematic design of the laser.

Laser diode and grating

The laser diode used in this setup [Eagleyard photonics, EYP-RWE-0790-0400-0750-SOT03-0000] has an anti-reflection coating. The effect of this coating is a broadening and blue shift of the gain spectrum of the semiconductor medium. The active region where the amplification takes place is confined to a thin middle layer. Above laser threshold, the carrier density depends on the ratio of the charge carriers that are generated by an applied current through the junction and the loss due to stimulated radiative transitions. Due to a reduction of the optical intensity, the number of charge carriers is increased and this leads to an enhancement of the band gap and thus, an enhanced gain in the blue end of the spectrum.

According to the manufacturer's specifications, the AR coated laser diode has a central wavelength of 770 nm and is tuneable from 750 nm to 790 nm. The desired potassium transition has a wavelength of 766,7 nm which is well in the range of the laser diode.

The grating used in this setup is a grating with 1800 grooves per mm [Thorlabs, GH13-18V]. It is adjusted such that the first order is used to inject the laser, while the zeroth order is leaves the laser case. The reflectivity of the first diffraction order depends on the orientation of the polarisation compared to the grating grooves.

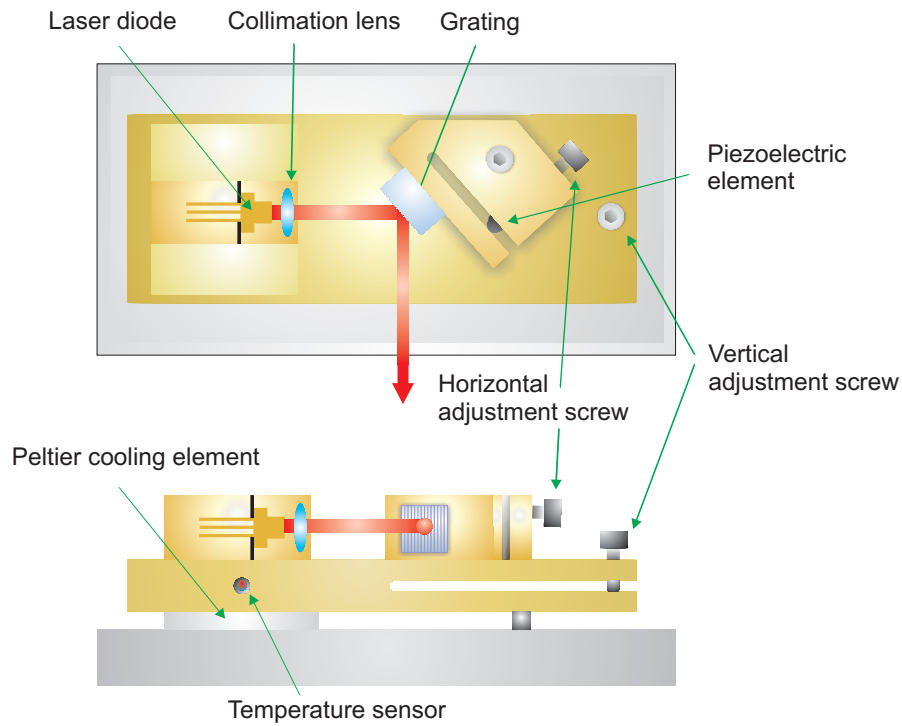


Figure 3.16: Schematic design of the laser.

Because of the anti reflection coating, the laser diode is very sensitive to high intensities and therefore, a low reflectivity of the first order is desired. This is achieved by adjusting the laser diode and the grating so that the emitted ellipse of laser light is parallel to the grating grooves. This way only few grooves contribute to the reflection, see figure 3.17.

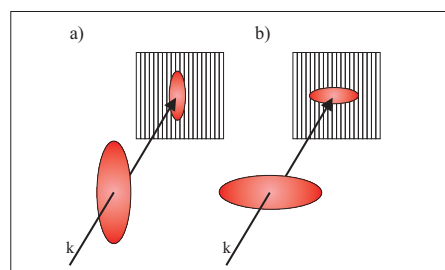


Figure 3.17: Orientation of the laser ellipse compared to the grating, a) for an AR coated laser diode, b) for a normal laser diode.

3.9.2 Laser current controller

The linewidth and the stability of a laser crucially depend on a reliable current source. Within the diploma project of C. Schubert [64], the performance of different laser current controllers was tested, with the result that the non-commercial laser controller designed by Libbrecht and Hall [55], proved to be the one with the lowest current noise and thus, achieved the narrowest laser linewidth. Therefore the formerly used laser controllers based on commercially available controller chips [Wavelength, LDD400-1P] were replaced.

The schematic circuit diagram is shown in appendix A. The high performance of the controller relies on high precision components with very low temperature coefficients that are used. A digital display that shows the desired current value greatly improved the adjustment of the current compared to the formerly used analog display for the current controller. It enables the reproducibility of a certain current value to set the laser frequency to the desired output.

The better performance of the new current controller becomes apparent when comparing a spectroscopic signal of ^{40}K using the two different controllers, see figure 3.18. It is the spectroscopy of the cooling transition of an ensemble of cold ^{40}K atoms at $1\mu\text{K}$ in the magnetic trap. The number of atoms is much more stable with the new controller and therefore provides a much higher reliability for measurements that are based on the particle number.

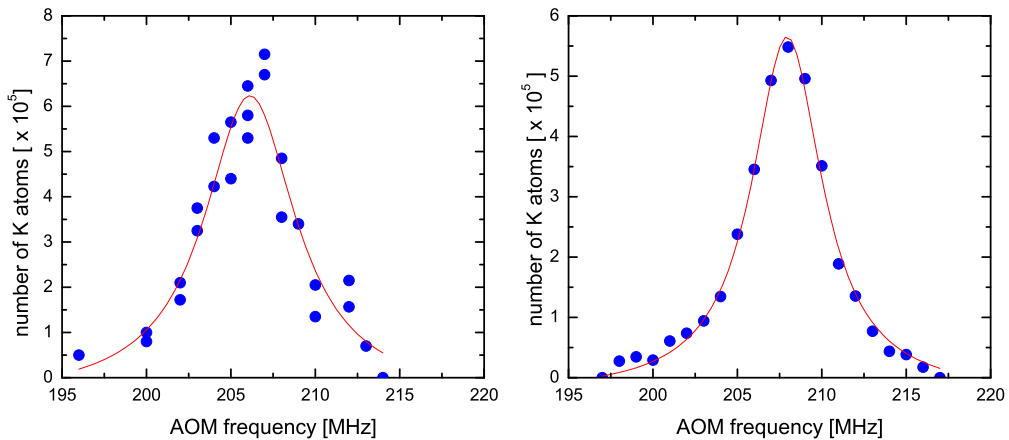


Figure 3.18: Comparison of a potassium spectroscopy signal. On the left measurement with the formerly used commercial laser current controller, on the right measurement with the new laser current controller.

How to address Rb atoms at high magnetic fields

As described in section 2.3, a way to produce ultracold heteronuclear molecules is by adjusting the scattering properties of colliding atoms via Feshbach resonances and create weakly bound molecules. These Feshbach molecules have a very short lifetime particularly due to collisional decay with the residual rubidium atoms [65, 66, 67].

Therefore it is necessary to develop a method to decrease the amount of rubidium atoms in the trap to enhance the lifetime of the molecules. This can be done by heating the atoms with resonant light until their kinetic energy is high enough that the atoms leave the trap. The problem is that the ^{87}Rb transitions are shifted by the magnetic field that is applied to produce the Feshbach molecules. This leads to a shift of the transition frequencies and the atoms are no longer resonant to the laser frequencies that are usually used for detecting the ^{87}Rb atoms.

Thus, a new laser system is needed that can address atoms even at high magnetic fields. The laser system that was built combines the efficiency of resonantly removing the atoms with a light pulse with the high selectivity of a microwave transition. This is necessary to avoid that the laser, here and in the following referred to as blast laser, is resonant with the Feshbach molecules and destroys them. The frequency of both blast laser and microwave can be freely adjusted to match the transition splitting at a broad range of possible magnetic fields. This makes the system a flexibly applicable instrument in addressing ^{87}Rb atoms at high magnetic fields.

The following sections explain the influence of the external magnetic field on the atomic states, how to calculate the new transition frequencies for ^{87}Rb at high magnetic fields and then give a detailed overview of the experimental setup of the blast laser system.

4.1 Interaction with an external magnetic field

In the presence of an external magnetic field the energy levels of the hyperfine structure split into magnetic sublevels in the presence of an external magnetic field. Therefore, the laser light used at low magnetic fields in a MOT will not be resonant anymore when a large magnetic field applied to the atoms as it is for forming Feshbach molecules. Hence, laser light at the new transition frequencies is needed.

Three regimes can be identified for increasing magnetic fields, the Zeeman regime for very weak magnetic field, an intermediate regime and the Paschen-Back regime for strong magnetic fields. Each of them is relevant for the calculation because the definition of weak and strong fields depends on the energy state in question.

Under the influence of a very weak external magnetic field, the hyperfine energy levels F split up into $2F + 1$ magnetic sublevels labelled with the quantum number m_F as indicated in figure 3.4. The energy splitting can be approximated with

$$\Delta E_{|F, m_F\rangle} = \mu_B g_F m_F B_z \quad (4.1)$$

where μ_B is the Bohr magneton, g_F the Landé g-factor, and B_z the external magnetic field component in z-direction. The energy splitting is proportional to the strength of the magnetic field.

For the intermediate region, the energy shift can in general only be calculated numerically as a diagonalization of the combined Hamiltonians of the hyperfine structure and the magnetic field interaction.

The exception is the case of a ground state with $J = 1/2$. It leads to the *Breit-Rabi formula* [68, 69]:

$$E_{|J=1/2, m_J, I, m_I\rangle} = -\frac{A_{hfs}(I + 1/2)}{2(2I + 1)} + g_I \mu_B m B \pm \frac{A_{hfs}(I + 1/2)}{2} \left(1 + \frac{4mx}{2I + 1} + x^2 \right)^{1/2}. \quad (4.2)$$

In this formula, A_{hfs} is the magnetic dipole constant, I the total nuclear angular momentum quantum number, $m = m_I \pm m_J = m_I \pm 1/2$ and $x = \frac{(g_J - g_I)\mu_B B}{A_{hfs}(I + 1/2)}$. It can be used to calculate the energy shifts for the ^{87}Rb ground state $5^2S_{1/2}$ for a certain magnetic field value. These energies are shown in figure 4.1.

In the Paschen-Back regime the hyperfine coupling between the total angular momentum of the electron \mathbf{J} and the nuclear angular momentum \mathbf{I} is weak compared to the coupling of \mathbf{I} and \mathbf{J} to the external field. This is the case either for a high magnetic field or for very weak hyperfine coupling for example in excited

states. Therefore it is the regime one has to look at when dealing with the excited ^{87}Rb state $5^2P_{3/2}$.

The good quantum numbers are now m_I and m_J , respectively the magnetic sub-level state of the nucleus and of the electron instead of F and m_F . The energy splitting can be calculated according to: [70, 69]

$$E_{|J,m_J,I,m_I\rangle} = A_{hfs}m_Jm_I + (g_Jm_J + g_I m_I)\mu_B B_z + B_{hfs} \frac{3(m_I m_J)^2 + \frac{3}{2}m_J m_I - I(I+1)J(J+1)}{2J(2J-1)I(2I-1)} \quad (4.3)$$

where B_{hfs} is the electric quadrupole constant.

It is possible to calculate the energy splittings for the magnetic sublevels of the excited $5^2P_{3/2}$ ^{87}Rb state at large magnetic field values.

4.1.1 Transition frequencies in the experiment

Figure 4.1 shows the splitted energy levels of the ^{87}Rb ground state $5^2S_{1/2}$ and the excited state $5^2P_{3/2}$ at a high magnetic field up to 600 G. One has to bear in mind that distance relations in this picture are adjusted to provide an overview and the real distance between the two states is still 780,241 nm. It can be seen that the ground state shows a linear splitting behaviour that is still consistent with the Zeeman regime whereas for the excited state, the energy splitting quickly merges to the Paschen-Back regime. This is because the hyperfine splitting of the excited state is much weaker and can therefore be broken more easily by an external magnetic field.

The transition that will be used to address the atoms at a high magnetic field is $|F = 2, m_F = 2\rangle \leftrightarrow |m'_I = 3/2, m'_J = 3/2\rangle$. The frequency of interest is detuning compared to the transition $|F = 2\rangle \leftrightarrow |F' = 3\rangle$ for $B = 0$. Evaluating the formulas of the previous section provides the needed values to calculate the transition for any magnetic field. This can be done with any scientific calculation program. The example case in figure 4.1 has been calculated for a magnetic field of 546,173 G. The evaluation of the formulas produces values of the energy splitting with respect to the fine state energy level. In figure 4.2 it is depicted how to obtain the actual detuning frequency. The difference of the fine to the hyperfine structure for $B = 0$ has to be subtracted from the value for the high magnetic field for both the ground and the excited state. These two differences again have to be subtracted. For the example case of 546,173 G, a detuning compared to the transition $|F = 2\rangle \leftrightarrow |F' = 3\rangle$ for $B = 0$ of 766,83 MHz is calculated.

A microwave is used for the transition between $|F = 1, m_F = 1\rangle \leftrightarrow |F = 2, m_F = 2\rangle$. For this transition, the evaluated values for the splitting of the ground state only have to be added. For 546,173 G, this is 8039,90 MHz.

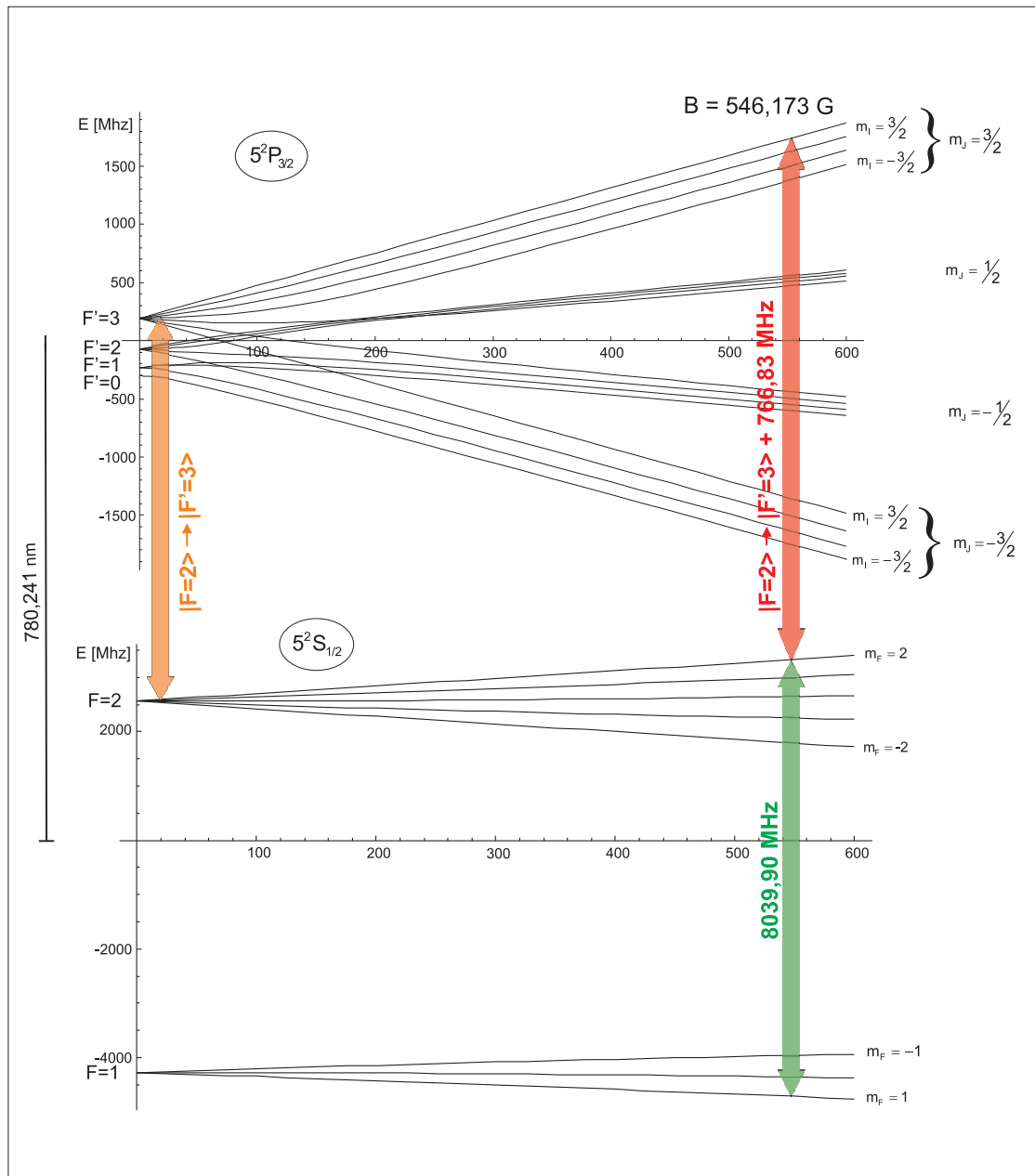


Figure 4.1: Level diagram of the ^{87}Rb atom for an external magnetic field.

4.2 Blast laser system with offset lock

In the following section, the blast laser system will be described. The new laser system that has been built up as a part of this master's thesis consists of three main parts. First the laser itself will be described. The second part describes how the laser is stabilized to the beat signal with the detection laser by an offset lock

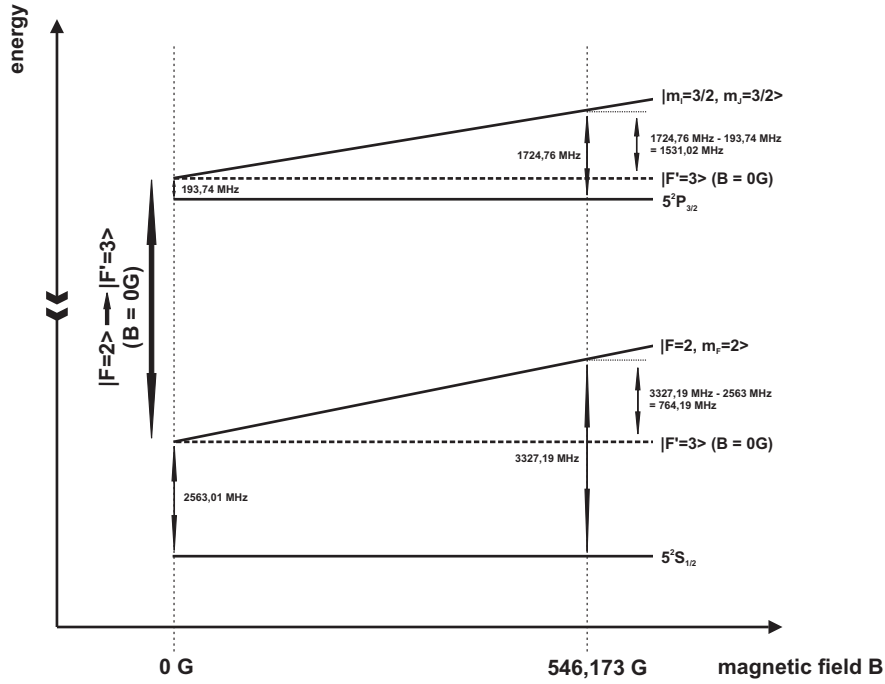


Figure 4.2: Example for the calculation of the detuning value.

to the exact desired value. The third part is the output, which includes an AOM double pass to tune the output laser frequency. Figure 4.3 shows the schematic illustration of the experimental set up.

4.2.1 Laser design

The Laser used in this system is identical to the one described in section 3.9.1. The laser diode (ADL-78901TX, Roithner LaserTechnik) is designed for a wavelength range from 775 nm to 795 nm with a peak wavelength of 785 nm. This model is used for CD players which makes it a cheap and reliable, commercially available device. The main difference to the setup described in section 3.9.1 is the non anti reflection coated laser diode. Therefore the orientation of the light ellipse has to be perpendicular to the grating grooves in order to reflect as much light in the first order to inject the laser as possible. This is the case for the right side of figure 3.17.

Linewidth approximation with beat signal

For the application of a laser in the experiment, it is important to know its linewidth. It is crucial for a measurement on an atomic transition that the laser

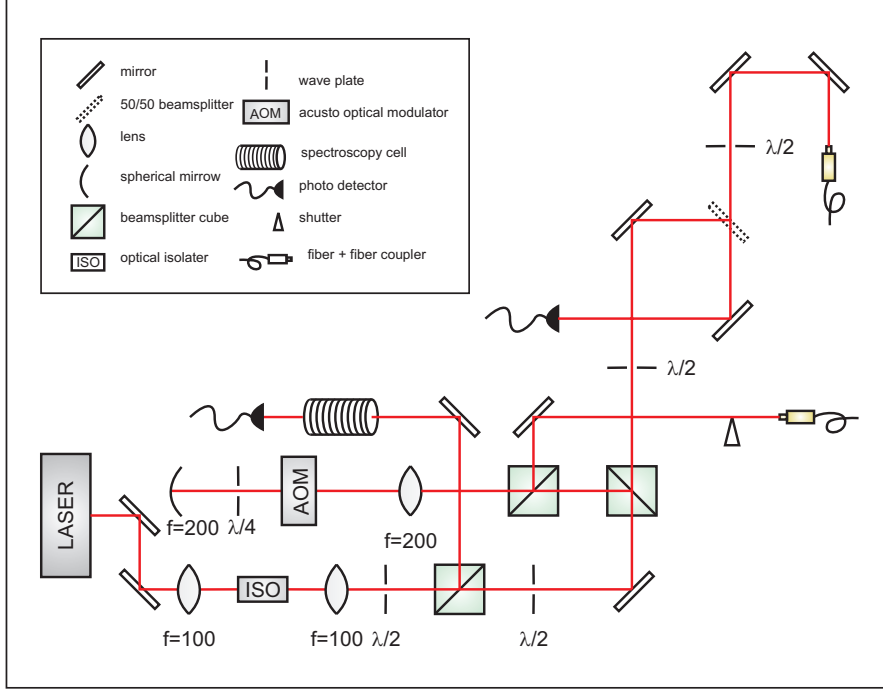


Figure 4.3: Schematic illustration of the laser system.

linewidth is significantly smaller than the transition itself. Whereas the natural linewidth of an atomic transition is defined by its life time, the linewidth of a laser is mainly limited by mechanical noise effects.

The ^{87}Rb transition $5^2S_{1/2} \rightarrow 5^2P_{3/2}$ that is addressed by the blast laser has a natural linewidth of 6,065 MHz [69].

To approximate the linewidth of the blast laser, a beat signal between the blast laser with the detection laser was recorded. A beat is the result of the superposition of two oscillations with similar frequencies. The simplest case to describe a beat mathematically is to consider two sine waves. The sum of two sine waves is

$$x_{sum} = a(\sin(2\pi f_1 t) + \sin(2\pi f_2 t)) \quad (4.4)$$

where a is the amplitude of the sum oscillation, and f_1 and f_2 are the frequencies of the two sine waves. With the sum-to-product identity follows

$$x_{sum} = 2a \sin\left(2\pi \frac{f_1 + f_2}{2} t\right) \cos\left(2\pi \frac{f_1 - f_2}{2} t\right). \quad (4.5)$$

The resulting beat frequency is

$$f_b = \frac{f_1 - f_2}{2}. \quad (4.6)$$

Measuring the beat signal to obtain information about the linewidth of the two lasers is based on the assumption that the linewidth of the beat signal is only caused

by the linewidth of the two lasers. It does not provide an independent linewidth for each laser, but it does provide an upper bound with which the linewidth can be approximated.

To measure the beat signal the blast laser and the detection laser were superimposed on a fast photodiode (Hamamatsu G4176). The resulting frequency spectrum is shown in figure 4.4.

To analyze the linewidth of the beat signal one has to bear in mind that it consists of two different contributions of noise. One follows a Lorentz profile:

$$L(\nu, w_L) = \frac{w_L/2\pi}{(\nu - \nu_0)^2 + (w_L/2)^2} \quad (4.7)$$

where $w_L = 2\gamma$ is the full width at half maximum (FWHM) of the Lorentz profile. The other contribution has a Gaussian profile:

$$G(\nu, w_G) = \frac{1}{\sigma\sqrt{2\pi}} e^{-\frac{(\nu-\nu_0)^2}{2\sigma^2}} \quad (4.8)$$

with a Gaussian FWHM of $w_G = 2\sigma\sqrt{2\ln(2)}$.

The combination of the two profiles in a convolution is called Voigt profile:

$$V(\nu, w_G, w_L) = \int d\nu' L(\nu - \nu', w_L) G(\nu', w_G) \quad (4.9)$$

This is the curve that has been fit to the measured beat signal.

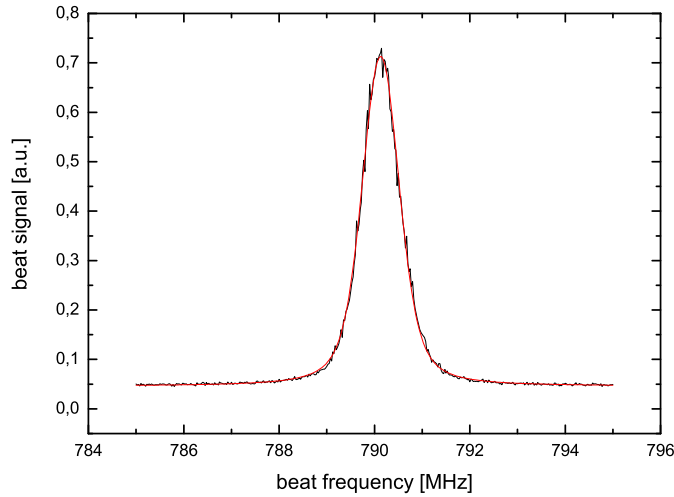


Figure 4.4: Beat signal with fitted voigt profile. The width of the Gaussian curve is $w_G=0,711$ MHz and the width of the Lorentzian curve is $w_L=0,377$.

The width of the Voigt profile can be approximated from the Gaussian and the Lorentzian width in an approximation that was first introduced by Olivero and

Longbothum, [71]

$$w_V \approx 0,5346w_L + \sqrt{0,2166w_L^2 + w_G^2}. \quad (4.10)$$

With the values for w_L and w_G that are extracted from figure 4.4, the linewidth for the beat signal is 1,112 MHz. This is only the upper bound of the linewidth and is still below the linewidth of the atomic transition of 6,065 MHz.

Spectroscopy

Absorption spectroscopy is used to preselect the wavelength that is later adjusted and stabilized by the offset lock. A small amount of light is sent through a glass cell with rubidium vapor. The glass cell is heated to increase the vapor pressure of the rubidium to amplify the signal. The signal is then recorded by a photo diode. To display the signal with an oscilloscope, the frequency of the blast laser is tuned over a small range with the piezo element that adjusts the position of the wavelength regulating grating in the laser. This is shown in figure 4.5.

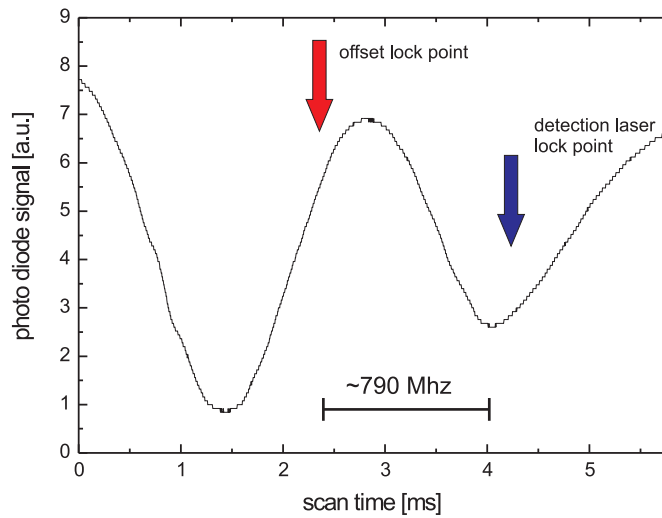


Figure 4.5: Doppler broadened spectroscopy signal. Indicated with red and blue arrows are the offset lock point and the detection laser lock point respectively.

4.2.2 Offset lock technique

The Offset lock is responsible for the stabilization of the blast laser at a frequency above the detection laser. This is achieved by converting the beat signal of the two lasers to a voltage signal, comparing it with an external adjustable reference voltage, and then stabilizing the blast laser with a PID controller.

A small part of the blast laser light is directed towards a fast photodetector (G4176-03, Hamamatsu Photonics, with a bias tee, PSPL 5545-107, EMCO Elektronik). There it is superimposed with light from the detection laser, that has been transferred to the blast laser system table by an optical fiber. The overlap of the two beams is crucial for the detection of a signal of the photo diode. It has been optimized during the setup phase by superimposing the two laser beams once over a long distance, before including the photodiode into the system. The obtained signal is the beat signal as described in section 4.2.1. Once a first signal has been obtained, it can be displayed with a spectrum analyzer, which makes the adjustment easier.

The signal of the photodiode is then fed into the offset-lock. Its circuit diagram is shown in appendix A. The main part of the offset lock is a frequency to voltage converter for the incoming frequency signal. Table 4.1 shows the conversion of different frequencies to the according voltage.

Frequency in MHz	Voltage in V
100	1,184
200	2,338
300	3,422
400	4,325
500	5,348
600	5,956
700	6,408
800	7,15
900	8,03
1000	8,31

Table 4.1: Frequency to voltage conversion of the offset lock.

This voltage is compared with an external reference voltage that can be adjusted between 0 and 12 V. With this reference voltage, the exact desired frequency can be set. The output of the offset lock circuit is the difference between this reference voltage and the converted signal voltage.

If the desired frequency difference between the two lasers is, for example, 793 MHz, the reference voltage has to be set to the corresponding voltage of 7,08 V. The laser will be adjusted manually to a value that is roughly the frequency of the transition $|F = 2\rangle \leftrightarrow |F' = 3\rangle$ plus the additional frequency of 793 MHz using the spectroscopy signal. This value will be displayed as the beat signal by the spectrum analyzer. In this case, the difference signal that is delivered by the offset lock circuit is roughly zero. If the laser frequency is higher, the difference is positive, if it is lower, the difference is negative. This signal is fed into a **proportional integral controller** (PI controller), which is connected to the piezo element of the laser and

which will then readjust the output frequency to the exact value.

Stability of the offset lock

The stability of the offset lock is a crucial factor in adjusting the frequency of the whole system. If the reference voltage source or the offset lock itself are not stable, the output will differ and so will the frequency to which the laser is locked. Thus, any fluctuations should be limited to values below the linewidth of the laser itself. An important improvement for the stability of the offset lock was the addition of a large heat sink to the electronic parts of the offset lock, because they proved to be very temperature sensitive.

The long term stability of the frequency to voltage conversion was tested by supplying a very precise frequency of 700 MHz to the offset lock. Without the reference voltage the output of the offset lock corresponds only to the conversion voltage. This voltage was measured directly at the output over a time of more than 2 hours. This measurement showed that the fluctuations are smaller than 10 mV which corresponds to a frequency of 1 MHz which roughly corresponds to the linewidth of the laser, see figure 4.6. Finally, the offset lock was tested for one hour in full operation with the beat signal as input frequency, while the lock frequency was measured with a spectrum analyzer. As expected, the fluctuations did not exceed 1 MHz.

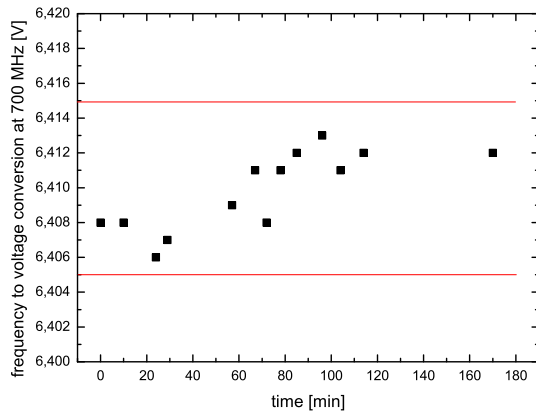


Figure 4.6: Fluctuations of the frequency to voltage conversion of the offset lock.

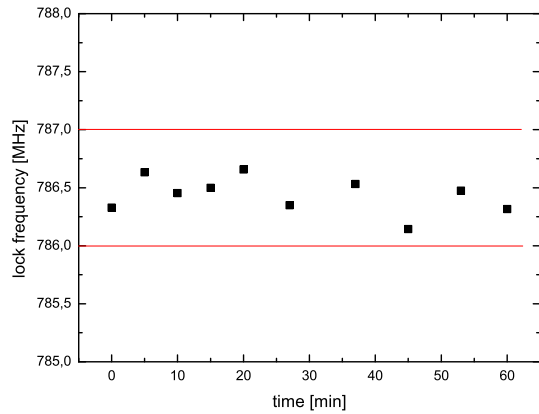


Figure 4.7: Fluctuations of the lock frequency.

4.2.3 Integration into the experiment

The main part of the laser light, after having split off some light for the spectroscopy and some for the offset lock, is almost ready for output. It has to pass

an AOM in double pass configuration and is then coupled into a fiber, that guides the light to the actual experimental site.

The AOM shifts the frequency of light using a sound wave. It splits the light into higher orders with the frequency of the sound wave added to these orders. The light is focussed with a lens ($f=200$ mm) on the AOM. After the first pass, all but the first order is blocked with a pinhole. The first order is then reflected by a spheric mirror ($f=200$ mm) back on the AOM. The second pass will deflect the first order back on the optical axis while again all other orders are blocked.

This way, an AOM that is driven by the frequency of 80 MHz, can detune the laser light 160 MHz in double pass configuration. The AOM can be used as a switch, because if it is turned off, no light at all will be in the first order. It can be used to scan the frequency of the laser of some tens of MHz.

Behind the AOM double pass the laser light is coupled into an optical fiber. This fiber transfers the light to the experimental. For its purpose of addressing and pushing away the atoms, the light does not have to be focused very tightly to the center of the glass cell where the atoms are located. It is sufficient for the blast laser light to shine onto the atomic ensemble. Therefore, no sophisticated optical setup is needed, the output fiber connector is mounted on the same height as the glass cell and the light is directed to the position of the atomic cloud. Figure 4.8 shows how the blast light is directed onto the atoms compared to the detection light.

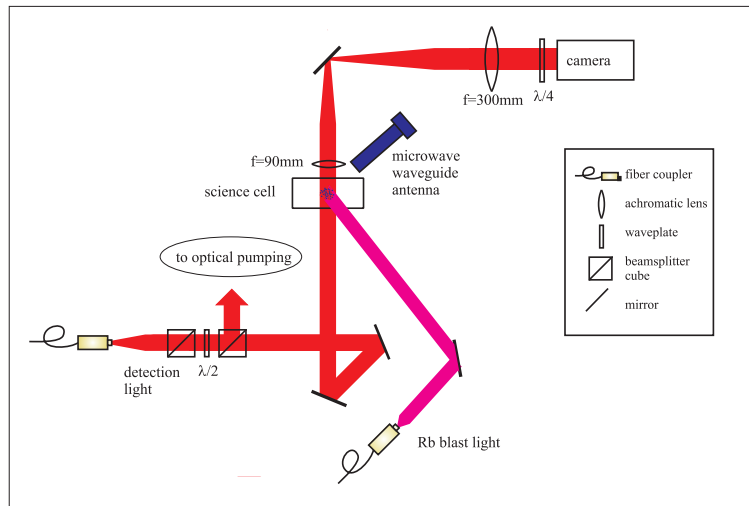


Figure 4.8: Schematic illustration of the adjustment of the blast light, the detection light and the microwave antenna to the atomic ensemble.

4.3 Microwave transition

The microwave is a crucial part in increasing the selectivity of the blast laser system. Since the microwave as well as the transition have extremely narrow linewidths, they provide a very precise instrument to address atoms. To avoid destruction of the weakly bound Feshbach molecules the linewidth has to be smaller than the binding energy of the molecules which is about 130 kHz. The transition addressed by the microwave has a linewidth of 12 kHz, as it will be shown in the result chapter 5.

For the transition from $|F = 1, m_F = 1\rangle$ to $|F = 2, m_F = 2\rangle$ a microwave of about 8 GHz is needed, as it was calculated in section 4.1.1. This microwave is generated in a cascade of different components, shown in figure 4.9. It was also used previously in this experiment for microwave evaporation where a 6,8 GHz microwave was needed [52, 72].

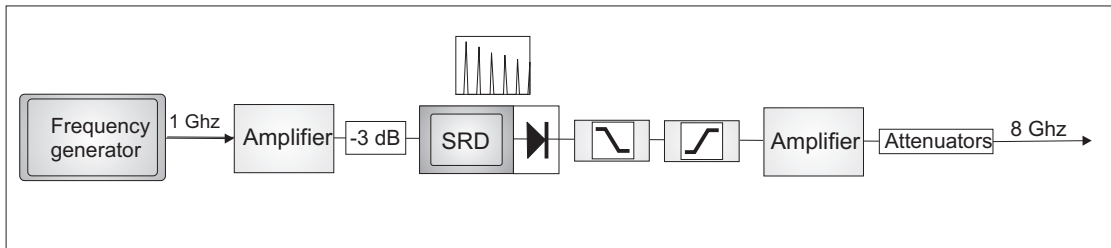


Figure 4.9: Generation process for the 8 GHz microwave.

A very precise frequency generator (Marconi Instruments signal generator 2024) is used to supply an initial signal of 1 GHz at -10 dBm. The signal is amplified by 27 dB and then attenuated for 3 dB to ensure that definitely no more than 0.5 W will enter the next important part of the chain, the step recovery diode comb harmonic generator.

This is a sensitive device generating higher harmonics of an input frequency. The step recovery diode used in this setup is a Herotek GC1000DC diode, specified for an input of 1000 MHz and 0,5 W. For the 7th harmonic it still has a specified output of up to 0 dBm. An integrated isolator helps to avoid the destruction of the diode due to back reflections.

To filter the 8 GHz out of the generated harmonics, a high pass filter (Minicircuits) is integrated to the chain. It suppresses all frequencies but 7900 - 11000 MHz. To improve the filter properties at lower frequencies, another low pass filter (Minicircuits VFL-7200+) is added that is suppresses from DC - 7200 MHz.

The filtered harmonic of 8 GHz is amplified up to 1 W with an amplifier (Minicircuits ZVE-8G) that is specified frequencies from 2000 to 8000 MHz.

The output power of the microwave can now adjusted by connecting additional

attenuators of the desired values. This is particularly important when the atom transition is analyzed to avoid power broadening.

Optimizing the microwave antenna

The microwave is directed to the atoms with a waveguide antenna (Omecon). A microwave is forming a standing wave inside the waveguide tube and the maximum output is reached when the end of the antenna is matched with an antinode of the standing microwave. This can be measured by recording the back reflection. The optimum output is reached for the smallest back reflection. To optimize the antenna length, small parts of the end were removed bit by bit and the reflection was detected. This optimization process is shown in figure 4.10.

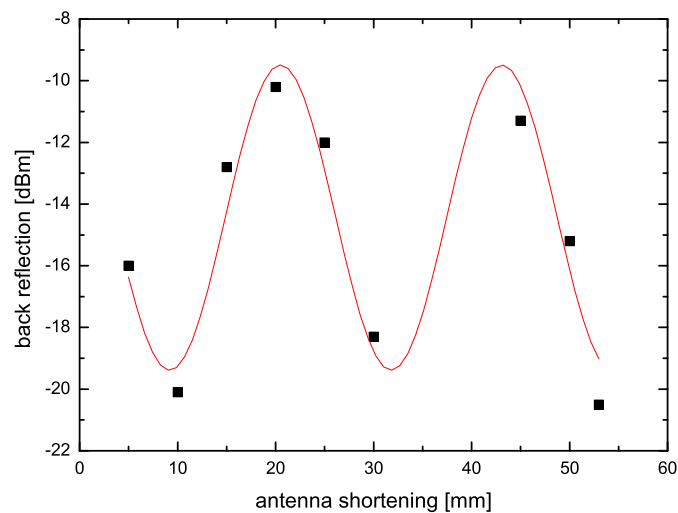


Figure 4.10: Shortening of the antenna tube to improve the output properties.

Characterization of the blast light laser system

The main purposes of the laser system that has been built within this master project are to be able to detect ^{87}Rb atoms at high magnetic fields and to remove the atoms from the trap to ensure the stability of ultracold Feshbach molecules. For the removal, a certain precision in addressing the atoms is needed to be sure not to affect the molecules. This is achieved by combining the laser system with a microwave that can address a transition with high selectivity.

In this chapter the results will be presented that have been achieved by applying the blast laser system and the microwave onto an ensemble of ^{87}Rb atoms. First it will be described how the parameters of the microwave that addresses the $|F = 1, m_F = 1\rangle$ to $|F = 2, m_F = 2\rangle$ transition are optimized. The next part will describe how atoms in the $|F = 2, m_F = 2\rangle$ state are removed by the laser light and subsequently the coupled system of microwave transition and laser light induced atom removal will be described. It will be shown that the narrow microwave transition in the coupled system does increase the selectivity of the removal process.

5.1 Microwave optimization

To obtain the optimum result in addressing the transition $|F = 1, m_F = 1\rangle$ to $|F = 2, m_F = 2\rangle$ at a high magnetic field, frequency and output power of the microwave have to be optimized.

By obtaining a spectroscopic signal of the transition, the center frequency at which most of the atoms are transferred can be determined. Figure 5.1 shows such a spectroscopy. The number of atoms in the $|F = 2, m_F = 2\rangle$ is detected. At a large detuning compared to the center frequency, almost no atoms can be detected which means that no atoms have been transferred. At the center frequency where

the microwave is resonant with the transition, most of the atoms are transferred to the $|F = 2, m_F = 2\rangle$ state. The center frequency for present spectroscopy was obtained by fitting a Gauss function to the measured data set. It is 8039,8924 MHz. The FWHM of the transition was determined to be 137,0 kHz.

As seen in section 3.8, the spectroscopic signal of the hyperfine transition can

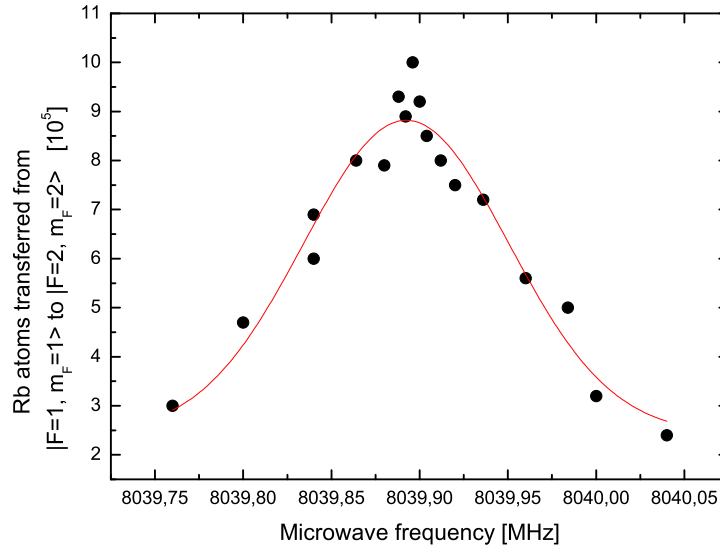


Figure 5.1: Transition between the hyperfine states $|F = 1, m_F = 1\rangle$ and $|F = 2, m_F = 2\rangle$ of ^{87}Rb at a magnetic field of 545,55 G. Center frequency of the Gauss fit is 8039.8923 MHz and FWHM is 137,0 kHz.

be used to determine the magnetic field. This was used to obtain a calibration for the current that generates the magnetic field. The current is used to set the magnetic field to the desired value, and each spectroscopy of the transition serves as a verification of this calibration and the actual magnetic field. The magnetic field value at which the transition shown in figure 5.1 was recorded is 545,55 G. The transition has been broadened due to the high microwave power. To obtain a narrower signal, the microwave power has to be reduced. This is achieved by connecting additional attenuators to the microwave generation chain that has been explained in section 4.3. As shown in figure 5.2 the width of the transition can be reduced considerably by attenuating the microwave power with -6 dB without reducing the amount of transferred atoms. The FWHM of transition with the unattenuated microwave is 137,0 kHz, whereas the attenuation of -6 dB leads to a FWHM of 97,1 kHz.

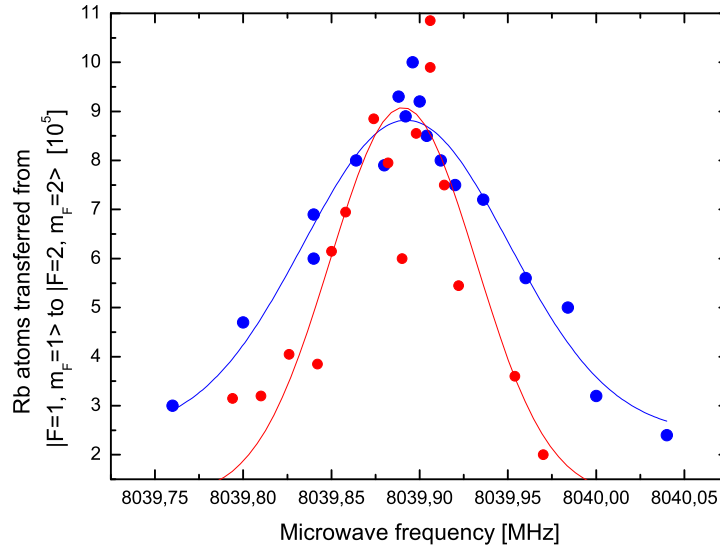


Figure 5.2: Spectroscopy signals of the $|F = 1, m_F = 1\rangle$ to $|F = 2, m_F = 2\rangle$ transition with different microwave output power. Blue dots represent no attenuation and red dots an attenuation of -6 dB. The blue Gauss curve fitted to the data has a FWHM of 137,0 kHz, and the red curve has a FWHM of 97,1 kHz.

5.2 Laser system optimization

The blast laser is used to remove the remaining atoms out of the dipole trap after the generation of Feshbach molecules. To do this, the transition $|F = 2, m_F = 2\rangle \leftrightarrow |m'_I = 3/2, m'_J = 3/2\rangle$ is addressed by the laser light. By obtaining the recoil energy of the photons that drive the transition, the atoms are gaining enough kinetic energy to leave the trap. The blast laser light needs to be resonant with the transition at a high magnetic field. Its frequency is set by the offset lock as well as by the AOM which the light passes before being directed to the atoms. It is convenient to set the offset lock to a fixed value, in this case 790 MHz, and scan the frequency of the AOM to obtain a signal. The atoms are detected in the $|F = 2, m_F = 2\rangle$ state. Scanning the frequency of the laser leads to a loss of atoms at the resonance frequency. This is shown in figure 5.3.

The blast laser is directed onto the atoms for 300 μs . It is then detected how many ^{87}Rb atoms were removed for which detuning of the AOM. The removal of ^{87}Rb atoms out of the trap is a dynamic process and therefore the linewidth of figure 5.3 cannot be identified with the linewidth of the transition. To avoid saturation the intensity was adjusted such that the atoms are not removed fully even at maximum.

The center frequency is determined to be 76 MHz for the AOM detuning. Together with the offset lock that has been set to 790 MHz, and twice the optimum AOM detuning frequency, taking into account the double pass configuration, the blast

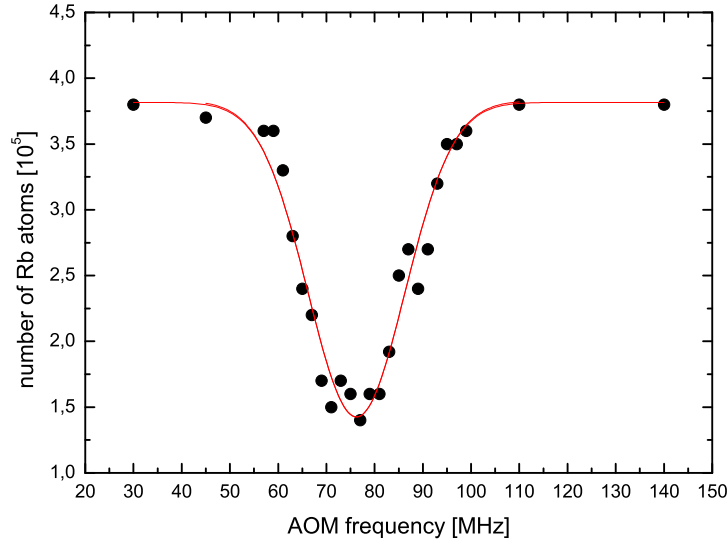


Figure 5.3: Removal of ^{87}Rb atoms, prepared in the $|F = 2, m_F = 2\rangle$ state, plotted against the detuning of the AOM frequency of the blast laser. The offset lock was set to a fixed frequency of 790 MHz, the pulse length was 300 μs , and the magnetic field was 545,956 G. The center frequency of the fitted Gauss curve is 76,24 MHz and the FWHM is 23,54 MHz.

laser frequency to remove the ^{87}Rb atoms at a magnetic field of 545,956 G is 942 MHz blue detuned compared to the detection laser.

The next step is to optimize the pulse length. To avoid the loss of Feshbach molecules due to collisions with the residual ^{87}Rb atoms, it is required to remove the atoms as fast as possible. Thus, the blast light pulse has to be as short as possible but with the maximum removal effect.

The optimization of the pulse length is shown in figure 5.4. For different pulse lengths, the amount of remaining ^{87}Rb atoms is measured. It is shown that for pulses that are too short, there are still ^{87}Rb atoms remaining in the trap. For a pulse duration of 300 μs , the atoms are fully removed.

5.3 Combination of laser and microwave

The combination of the highly selective microwave transition with the high efficiency of ^{87}Rb atom removal through the resonant laser at high magnetic fields is desired. Therefore, both the microwave and the laser are directed onto the atoms together, for a combined pulse.

Figure 5.5 shows the combined process. The black dots represent the loss of ^{87}Rb atoms that is achieved by applying the combination of microwave and laser to the atoms. The laser frequency is fixed to a total offset of $788\text{MHz} + 2 \cdot 74\text{MHz} = 936\text{MHz}$. This is the optimum removal frequency for a magnetic field of 546,2 G.

In comparison, the red dots in figure 5.5 belong to the transition $|F = 1, m_F = 1\rangle$ to $|F = 2, m_F = 2\rangle$ that is purely addressed by the microwave. It indicates how many atoms are transferred and it has a width of 91,1 kHz.

For a non-coupled process, where the atoms are independently transferred from $|F = 1, m_F = 1\rangle$ to $|F = 2, m_F = 2\rangle$ and then removed by the blast laser light, one would expect that scanning over the microwave transition with fixed blast light would lead to the same width as the pure microwave transition. Figure 5.5 clearly shows that this is not the case and the process is coupled.

To examine this coupling more closely, the dependence of the selectivity on the intensity of the laser light was measured. The selectivity of the combined system can be increased even more by reducing the laser power, as it is shown in figure 5.6. The values that show the selectivity are compared to each other in table 5.1. Plotting the selectivity against the blast laser intensity shows linear characteris-

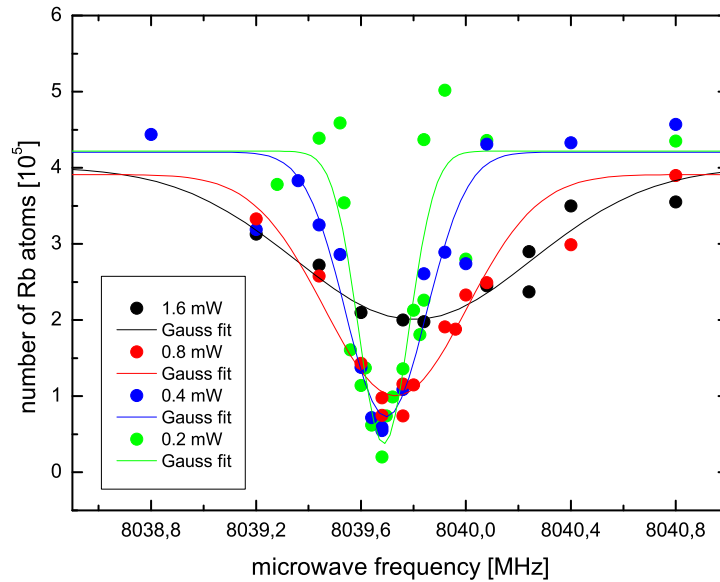


Figure 5.6: Reduction of the laser power to increase the selectivity of the atom removal. The values for the linewidths of the fitted Gaussian profiles are shown in table 5.1.

tics, see figure 5.7. The data is fitted with a linear function that has a zero offset of 106,2 MHz. This value corresponds within the error range to the linewidth of the pure microwave transition that was 91,2 MHz. Note that the microwave transition is plotted in figure 5.7 as a red dot but has not been included in fitting the data points to a linear function. Thus, figure 5.7 depicts the linear behavior of the coupling with increasing laser light intensity.

Linewidth of the pure microwave transition	91,1 kHz
Selectivity of the pure laser system	23000 kHz
Selectivity of the combined system:	
Laser power	Selectivity
1,6 mW	1064,4 kHz
0,8 mW	636,7 kHz
0,4 mW	363,2 kHz
0,2 mW	227,7 kHz

Table 5.1: Comparison of the selectivity of the combined laser and microwave system

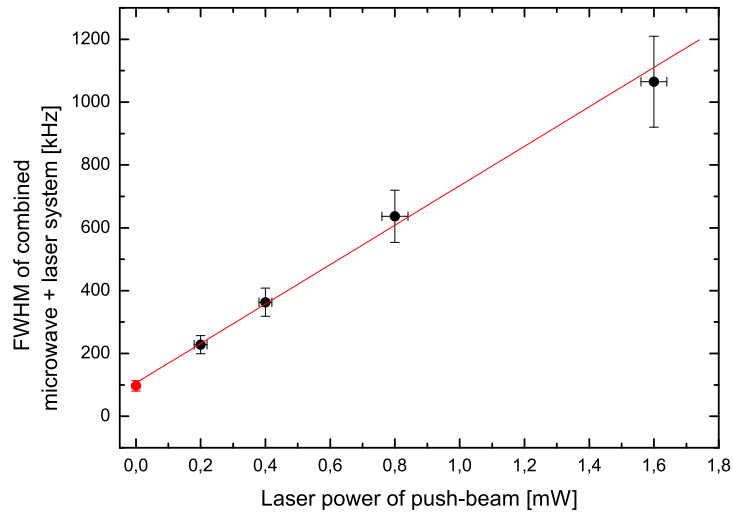


Figure 5.7: Reduction of the laser power to increase the selectivity of the atom removal. The linear function was fitted only to the black dots, representing the combined system of laser and microwave and has an zero offset of 106,2 MHz. The red dot represents the linewidth of the pure microwave transition of 91,2 MHz.

5.4 Conclusion

In conclusion, the optimum values for operating the blast laser system in combination with the microwave are summarized.

The values for adjusting the frequency of both blast laser and microwave depend on the applied magnetic field and can be calculated following section 4.1.1. As an example, for a magnetic field of 546,057 G, the microwave has to be set to 8039,640 MHz, and the offset of the laser compared to the detection laser has to be set to 790 MHz for the offset lock and 76 MHz for the AOM. This corresponds to a total

offset of $790 \text{ MHz} + 2.76 = 942 \text{ MHz}$. The microwave power has to be attenuated with -6dB. The output of the laser is 0,08 mW which corresponds to a selectivity value according to figure 5.7 of 160 MHz. The combined laser light plus microwave pulse is applied to the atoms for $300 \mu\text{s}$.

The system has been tested as a part of the experimental operation sequence in generating KRb Feshbach molecules and has proved its ability in increasing the lifetime of the molecules by reliably removing ^{87}Rb atoms at high magnetic fields.

Chapter 6

Outlook

Experiments with ultracold $^{40}\text{K}^{87}\text{Rb}$ molecules offer promising perspectives for the research of dipolar interactions in many particle systems. This thesis presents a laser system for these experiments which enhances the lifetime of these molecules. This is a prerequisite for the transfer of the highly excited Feshbach molecules to the deeply bound ground state.

The laser system is an inherent part of the experiment used to remove residual rubidium atoms to stabilize the Feshbach molecules. In addition this system can be used to detect the number of rubidium atoms at high magnetic fields. This provides another way to detect the production of molecules. In such a detection scheme, the molecules are dissociated by applying a microwave pulse that transfers the ^{87}Rb atoms from $|F = 1, m_F = 1\rangle$ to $|F = 2, m_F = 2\rangle$. This microwave pulse has to have the energy needed to transfer free atoms plus the binding energy of the molecules. By scanning the microwave frequency and detecting the number of atoms it is possible to measure the molecular binding energy.

Having achieved stable Feshbach molecules, the next step is to transfer the molecules to a low vibrational state. The ultimate goal of this work is to produce ultracold polar molecules to examine the anisotropic dipole interaction in such a sample. Being able to create ground state KRb molecules would lead to a polar molecule that could be easily aligned with an electric field.

The transfer can be realized by using a stimulated Raman adiabatic passage (STIRAP) [73]. This method has recently been used on a similar system in the group of D. Jin, [74]. It uses a three level scheme to transfer the molecules to the desired state. By coupling the final state with an intermediate excited state with a laser, a coherent superposition of the two initially unpopulated states is obtained. Coupling this superposition with the pump laser to the initial state, the population is

transferred directly to the final state, avoiding loss due to decay from the excited intermediate state.

The experimental realization requires some preliminary work. Franck-Condon factors indicating the transition probability to excited states have already been calculated by the group of E. Tiemann and an appropriate three level system has been identified theoretically. The next step is to determine these states spectroscopically. With these prerequisites, a successful STIRAP transfer can be performed and KRb ground state molecules can be generated.

Appendix A

Circuit diagrams

The circuit diagrams of the current controller A.1 and the frequency-to-voltage converter for the offset lock A.2 are presented.

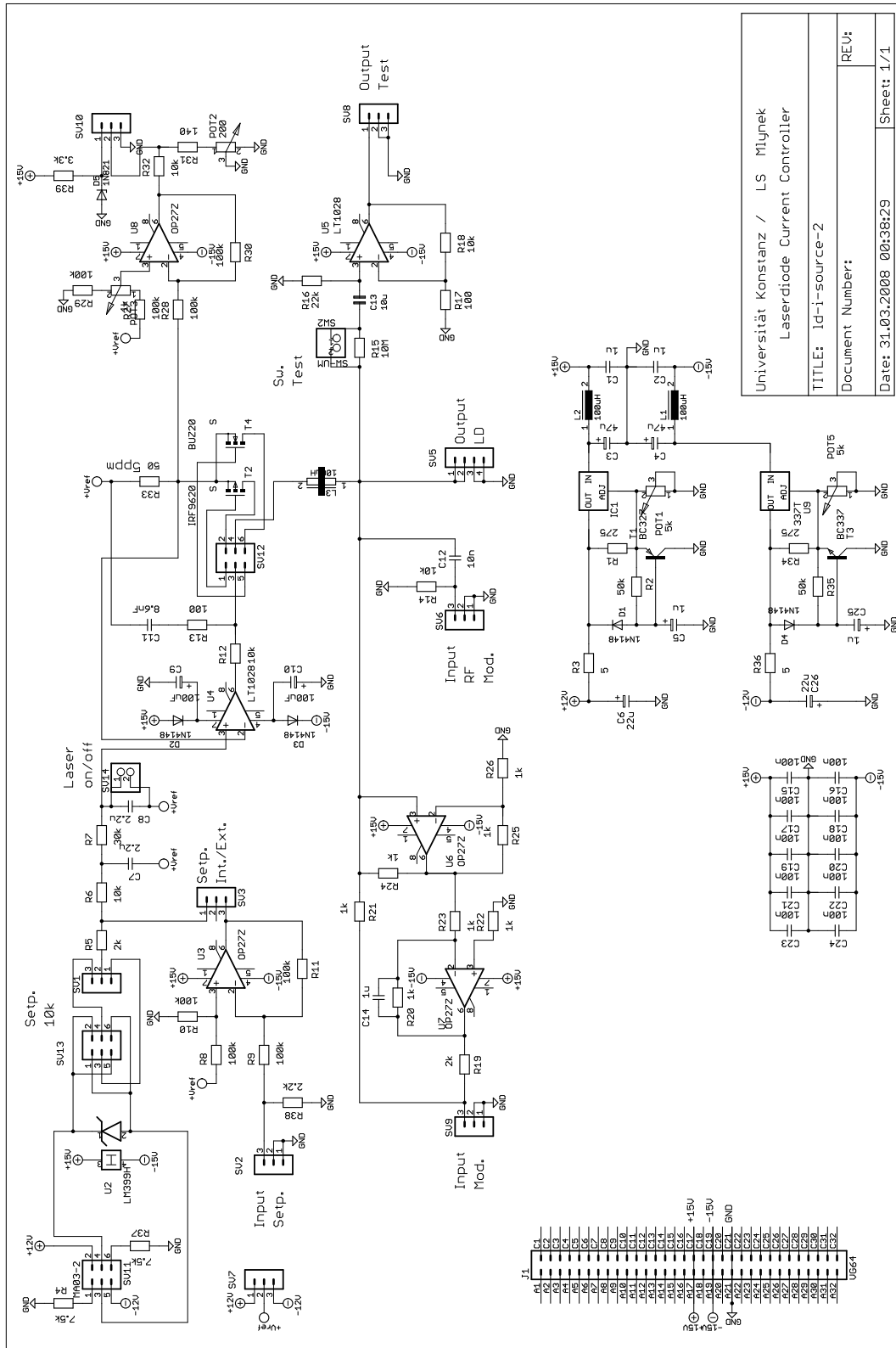


Figure A.1: Circuit diagram of the current controller.

Universität Konstanz / LS Mlynek
 Laserdiode Current Controller
 TITLE: Id-i-source-2
 Document Number:
 Date: 31.03.2008 00:38:29
 Sheet: 1/1

Bibliography

- [1] Goethe, J. W.: *Faust*.
C.H. Beck, Muenchen (1998).
- [2] Planck, M.: *Zur Theorie des Gesetzes der Energieverteilung im Normalspektrum*.
Verhandlungen der Deutschen Physikalischen Gesellschaft **2**, 237–245 (1900).
- [3] Kozlov, M. G. and Labzowsky, L. N.: *Parity violation effects in diatomics*.
J. Phys. B: A. Mol. Opt. Phys. **28**, 1993 (1995).
- [4] Stuhler, J., Griesmaier, A., Koch, T., Fattori, M., Pfau, T., Giovanazzi, S.,
Pedri, P. and Santos, L.: *Observation of Dipole-Dipole Interaction in a
Degenerate Quantum Gas*.
Phys. Rev. Lett. **95**(15), 150406 (2005).
- [5] Giovanazzi, S., Pedri, P., Santos, L., Griesmaier, A., Fattori, M., Koch, T.,
Stuhler, J. and Pfau, T.: *Expansion dynamics of a dipolar Bose-Einstein
condensate*.
Phys. Rev. A **74**(1), 013621 (2006).
- [6] DeMille, D.: *Quantum Computation with Trapped Polar Molecules*.
Phys. Rev. Lett. **88**(6), 067901 (2002).
- [7] Bose, S.: *Plancks Gesetz und Lichtquantenhypothese*.
Z. Phys. **26**(1), 178–181 (1924).
- [8] Einstein, A.: *Quantentheorie des idealen einatomigen Gases*.
Sitzber. Kgl. Preuss. Akad. Wiss., Phys. Math. Kl. Bericht **22**, 261 (1924).
- [9] Einstein, A.: *Quantentheorie des idealen einatomigen Gases II*.
Sitzber. Kgl. Preuss. Akad. Wiss., Phys. Math. Kl. Bericht **3**, 18 (1925).
- [10] Pauli, W.: *Über den Zusammenhang des Abschlusses der Elektronengruppen
im Atom mit der Komplexstruktur der Spektren*.
Z. Phys. **31**, 765 (1925).
- [11] Pauli, W.: *Exclusion principle and quantum mechanics*.
Nobel lecture, 13. December 1945.

-
- [12] Fermi, E.: *Zur Quantelung des idealen einatomigen Gases.*
Z. Phys. **36**(11), 902–912 (1926).
- [13] Pauli, W.: *The Connection Between Spin and Statistics.*
Phys. Rev. **58**(8), 716–722 (1940).
- [14] London, F.: *On the Bose-Einstein condensation.*
Phys. Rev. **54**(11), 947–954 (1938).
- [15] London, F.: *The λ -Phenomenon of Liquid Helium and the Bose-Einstein Degeneracy.*
Nature **141**, 643 (1938).
- [16] Lebedev, P.: *The experimental study of the pressure of light.*
Ann. Phys. **6**, 433 (1901).
- [17] Hänsch, T. W. and Schalow, A. L.: *Cooling of gases by laser radiation.*
Opt. Comm. **13**, 68–69 (1975).
- [18] Raab, E. L., Prentiss, M., Cable, A., Chu, S. and Pritchard, D. E.: *Trapping of Neutral Sodium Atoms with Radiation Pressure.*
Phys. Rev. Lett. **59**(23), 2631–2634 (1987).
- [19] Lett, P. D., Watts, R. N., Westbrook, C. I., Phillips, W. D., Gould, P. L. and Metcalf, H. J.: *Observation of Atoms Laser Cooled below the Doppler Limit.*
Phys. Rev. Lett. **61**(2), 169–172 (1988).
- [20] Dalibard, J. and C., Cohen-Tannoudji: *Laser cooling below the Doppler limit by polarization gradients: simple theoretical models.*
J. Opt. Soc. Am. B **6**, 2023 (1989).
- [21] Hess, H. F.: *Evaporative cooling of magnetically trapped and compressed spin-polarized hydrogen.*
Phys. Rev. B **34**, 3476–3479 (1986).
- [22] Anderson, M. H., Ensher, J. R., Matthews, M. R., Wieman, C. E. and Cornell, E. A.: *Observation of Bose-Einstein Condensation in a Dilute Atomic Vapor.*
Science **269**(5221), 198 (1995).
- [23] Davis, K. B., Mewes, M. O., Andrews, M. R., Druten, N. J. van, Durfee, D. S., Kurn, D. M. and Ketterle, W.: *Bose-Einstein Condensation in a Gas of Sodium Atoms.*
Phys. Rev. Lett. **75**(22), 3969–3973 (1995).
- [24] DeMarco, B. and Jin, D. S.: *Onset of Fermi Degeneracy in a Trapped Atomic Gas.*
Science **285**(5434), 1703–1706 (1999).

-
- [25] DeMarco, B., Rohner, H. and Jin, D.S.: *An enriched ^{40}K source for fermionic atom studies.*
Rev. Scient. Instr. **70**(4), 1967–1969 (1999).
- [26] Schreck, F., Khaykovich, L., Corwin, K. L., Ferrari, G., Bourdel, T., Cubizolles, J. and Salomon, C.: *Quasipure Bose-Einstein Condensate Immersed in a Fermi Sea.*
Phys. Rev. Lett. **87**(8), 080403 (2001).
- [27] Truscott, A. G., Strecker, K. E., McAlexander, W. I., Partridge, G. B. and Hulet, R. G.: *Observation of Fermi Pressure in a Gas of Trapped Atoms.*
Science **291**(5513), 2570–2572 (2001).
- [28] Hadzibabic, Z., Stan, C. A., Dieckmann, K., Gupta, S., Zwierlein, M. W., Görlitz, A. and Ketterle, W.: *Two-Species Mixture of Quantum Degenerate Bose and Fermi Gases.*
Phys. Rev. Lett. **88**(16), 160401 (2002).
- [29] Roati, G., Riboli, F., Modugno, G. and Inguscio, M.: *Fermi-Bose Quantum Degenerate ^{40}K – ^{87}Rb Mixture with Attractive Interaction.*
Phys. Rev. Lett. **89**(15), 150403 (2002).
- [30] Feshbach, H.: *Unified Theory of Nuclear Reactions.*
Rev. Mod. Phys. **36**(4), 1076–1078 (1964).
- [31] Inouye, S., Andrews, MR, Stenger, J., Miesner, HJ, Stamper-Kurn, DM and Ketterle, W.: *Observation of Feshbach resonances in a Bose-Einstein condensate.*
Nature **392**(6672), 151–154 (1998).
- [32] Loftus, T., Regal, C. A., Ticknor, C., Bohn, J. L. and Jin, D. S.: *Resonant Control of Elastic Collisions in an Optically Trapped Fermi Gas of Atoms.*
Phys. Rev. Lett. **88**(17), 173201 (2002).
- [33] Donley, E. A., Claussen, N. R., Thompson, S. T. and Wieman, C.: *Atom-molecule coherence in a Bose-Einstein condensate.*
Nature **417**, 529–533 (2002).
- [34] Regal, C. A., Ticknor, C., Bohn, J. L. and Jin, D. S.: *Creation of ultracold molecules from a Fermi gas of atoms.*
Nature **424**(6944), 47–50 (2003).
- [35] Jochim, S., Bartenstein, M., Altmeyer, A., Hendl, G., Chin, C., Denschlag, J. Hecker and Grimm, R.: *Pure Gas of Optically Trapped Molecules Created from Fermionic Atoms.*
Phys. Rev. Lett. **91**(24), 240402 (2003).
- [36] Cubizolles, J., Bourdel, T., Kokkelmans, S. J., Shlyapnikov, G. V. and Salomon, C.: *Production of Long-Lived Ultracold Li_2 Molecules from a Fermi Gas.*

- Phys. Rev. Lett. **91**(24), 240401 (2003).
- [37] Greiner, M., Regal, C. A. and Jin, D. S.: *Emergence of a molecular Bose-Einstein condensate from a Fermi gas.*
Nature **426**(6966), 537–540 (2003).
- [38] Zwierlein, M. W., Stan, C. A., Schunck, C. H., Raupach, S. M. F., Gupta, S., Hadzibabic, Z. and Ketterle, W.: *Observation of Bose-Einstein Condensation of Molecules.*
Phys. Rev. Lett. **91**(25), 250401 (2003).
- [39] Bardeen, J., Cooper, L. N. and Schrieffer, J. R.: *Theory of Superconductivity.*
Phys. Rev. **108**(5), 1175–1204 (1957).
- [40] Regal, C. A., Greiner, M. and Jin, D. S.: *Lifetime of Molecule-Atom Mixtures near a Feshbach Resonance in K.*
Phys. Rev. Lett. **92**(8), 083201 (2004).
- [41] Bourdel, T., Khaykovich, L., Cubizolles, J., Zhang, J., Chevy, F., Teichmann, M., Tarruell, L., Kokkelmans, S. J. J. M. F. and Salomon, C.: *Experimental Study of the BEC-BCS Crossover Region in ^6Li .*
Phys. Rev. Lett. **93**(5), 050401–4 (2004).
- [42] Kinast, J., Hemmer, S. L., Gehm, M. E., Turlapov, A. and Thomas, J. E.: *Evidence for Superfluidity in a Resonantly Interacting Fermi Gas.*
Phys. Rev. Lett. **92**(15), 150402–4 (2004).
- [43] Zwierlein, M. W., Stan, C. A., Schunck, C. H., Raupach, S. M. F., Kerman, A. J. and Ketterle, W.: *Condensation of Pairs of Fermionic Atoms near a Feshbach Resonance.*
Phys. Rev. Lett. **92**(12), 120403–4 (2004).
- [44] Modugno, M., Ferlaino, F., Riboli, F., Roati, G., Modugno, G. and Inguscio, M.: *Mean-field analysis of the stability of a K-Rb Fermi-Bose mixture.*
Phys. Rev. A **68**(4), 043626 (2003).
- [45] Pezze, L., Pitaevskii, L., Smerzi, A., Stringari, S., Modugno, G., Mirandes, E. de, Ferlaino, F., Ott, H., Roati, G. and Inguscio, M.: *Insulating Behavior of a Trapped Ideal Fermi Gas.*
Phys. Rev. Lett. **93**(12), 120401–4 (2004).
- [46] Gunter, K., Stöferle, T., Moritz, H., Köhl, M. and Esslinger, T.: *p-Wave Interactions in Low-Dimensional Fermionic Gases.*
Phys. Rev. Lett. **95**(23), 230401–4 (2005).
- [47] Köhl, M., Moritz, H., Stöferle, T., Gunter, K. and Esslinger, T.: *Fermionic Atoms in a Three Dimensional Optical Lattice: Observing Fermi Surfaces, Dynamics, and Interactions.*
Phys. Rev. Lett. **94**(8), 080403–4 (2005).

-
- [48] Rom, T., Best, Th., Oosten, D. van, Schneider, U., Folling, S., Paredes, B. and Bloch, I.: *Free fermion antibunching in a degenerate atomic Fermi gas released from an optical lattice.*
Nature **444**(7120), 733–736 (2006).
- [49] Ott, H., Mirandes, E. de, Ferlaino, F., Roati, G., Modugno, G. and Inguscio, M.: *Collisionally Induced Transport in Periodic Potentials.*
Phys. Rev. Lett. **92**(16), 160601–4 (2004).
- [50] Ospelkaus, S., Ospelkaus, C., Wille, O., Succo, M., Ernst, P., Sengstock, K. and Bongs, K.: *Localization of Bosonic Atoms by Fermionic Impurities in a Three-Dimensional Optical Lattice.*
Phys. Rev. Lett. **96**(18), 180403 (2006).
- [51] Papp, S. B. and Wieman, C. E.: *Observation of Heteronuclear Feshbach Molecules from a ^{85}Rb - ^{87}Rb Gas.*
Phys. Rev. Lett. **97**(18), 180404 (2006).
- [52] Klempt, C.: *Wechselwirkung in Bose-Fermi-Quantengasen.*
PhD thesis, Leibniz Universität Hannover (2007).
- [53] Topic, O.: *Präparation einer ultrakalten Bose-Fermi Mischung.*
Diploma thesis, Leibniz Universität Hannover (2005).
- [54] Will, J.: *Realisierung einer magneto-optischen Falle für ^{41}K .*
Diploma thesis, Leibniz Universität Hannover (2007).
- [55] Libbrecht, K.L. and Hall, J. L.: *A low-noise high-speed diode laser current controller.*
Rev. Scient. Instr. **64**(8), 2133 (1993).
- [56] Klempt, C., Zoest, T. van, Henninger, T., Topic, O., Rasel, E., Ertmer, W. and Arlt, J.: *Ultraviolet light-induced atom desorption for large rubidium and potassium magneto-optical traps.*
Phys. Rev. A **73**(1), 13410 (2006).
- [57] Majorana, E.: *Atomi orientati in campo magnetico variabile.*
Nuovo cimento **9**, 43–50 (1932).
- [58] Esslinger, T., Bloch, I. and Hänsch, T. W.: *Bose-Einstein condensation in a quadrupole-Ioffe-configuration trap.*
Phys. Rev. A **58**(4), R2664–R2667 (1998).
- [59] Klempt, C., Henninger, T., Topic, O., Will, J., Falke, St., Ertmer, W. and Arlt, J.: *Transport of a quantum degenerate heteronuclear Bose-Fermi mixture in a harmonic trap.*
arXiv:0708.2845 (2007).
- [60] Ashkin, A.: *Trapping of atoms by resonance radiation pressure.*
Phys. Rev. Lett. **40**, 729–732 (1978).

-
- [61] Ashkin, A., Dziedzic, J. M., Bjorkholm, J. E. and Chu, S.: *Observation of a single-beam gradient force optical trap for dielectric particles.* Opt. Lett. **11**, 288–290 (1986).
- [62] Grimm, R., Weidemüller, M. and Ovchinnikov, Y. B.: *Optical dipole traps for neutral atoms.* Adv. At. Mol. Opt. Phys. **42**, 95 (2000).
- [63] Ricci, L., Weidemüller, M., Esslinger, T., Hemmerich, A., Zimmermann, C., Vuletic, V., König, W. and Hänsch, T. W.: *A compact grating-stabilized diode laser system for atomic physics.* Opt. Comm. **117**, 541–549 (1995).
- [64] Schubert, C.: *Realisierung eines schmalbandigen Lasersystems hoher Ausgangsleistung für Präzisionsmessungen an ^{87}Rb .* Diploma thesis, Leibniz Universität Hannover (2007).
- [65] Xu, K., Mukaiyama, J. R., Abo-Shaeer, J. R., Chin, J. K., Miller, D. E. and Ketterle, W.: *Formation of quantum degenerate sodium molecules.* Phys. Rev. Lett. **91**(21), 210402 (2003).
- [66] Thalhammer, G., Winkler, K., Lang, F., Schmid, S., Grimm, R. and Denschlag, J. Hecker: *Long-Lived Feshbach Molecules in a Three-Dimensional Optical Lattice.* Phys. Rev. Lett. **96**(5), 050402 (2006).
- [67] N., Syassen, T., Volz, S., Teichmann, S., Dürr and Rempe, G.: *Collisional decay of ^{87}Rb Feshbach molecules at 1005,8 G.* Phys. Rev. A **74** (2006).
- [68] Breit, G. and Rabi, I. I.: *Measurement of Nuclear Spin.* Phys. Rev. **38**(11), 2082–2083 (1931).
- [69] Steck, D.A.: *Rubidium 87 D Line Data.* Tech. report, Los Alamos National Laboratory (2001).
- [70] E. B. Alexandrov, M. P. Chaika, G. I. Khvostenko: *Interference of Atomic States.* Springer-Verlag, Berlin (1993).
- [71] Olivero, J. J. and Longbothum, R. L.: *Empirical Fits to the Voigt Line Width: A Brief Review.* J. Quant. Spectrosc. Radiat. Transfer **17**, 233–236 (1977).
- [72] Gilowski, M.: *Aufbau und Charakterisierung eines Raman-Lasersystems zur Sagnac-Interferometrie mit kalten Atomen.* Diploma thesis, Leibniz Universität Hannover (2005).
- [73] Bergmann, K., Theuer, H. and Shore, B. W.: *Coherent population transfer among quantum states of atoms and molecules.* Rev. Mod. Phys. **70**, 1003–1025 (1998).

-
- [74] Ospelkaus, S., Pe'er, A., K.-K., Ni, Zirbel, J. J., Neyenhuis, B., Kotochigova, S., Julienne, P., Ye, J. and Jin, D. S.: *Ultracold dense gas of deeply bound heteronuclear molecules*.
arXiv:0802.1093 (2008).

List of Figures

2.1	The different behavior of bosons and fermions at ultracold temperatures.	4
2.2	Zero temperature Fermi distribution	8
3.1	Magneto-optical trap with magnetic coils in anti Helmholtz configuration and six laser beams.	14
3.2	Illustration of the velocity dependence of the force, for a red detuned laser.	15
3.3	Schematic illustration of the energy level shift for a applied magnetic field B	16
3.4	^{87}Rb fine and hyperfine structure with indicated laser transitions . .	17
3.5	^{40}K fine and hyperfine structure with indicated laser transitions . .	17
3.6	Schematic illustration of the lasersystem.	18
3.7	Schematic illustration of the vacuum system [53].	19
3.8	Scheme of magnetic trap in QUIC configuration. It consists of two quadrupole coils in anti Helmholtz configuration and an additional QUIC coil. The yellow arrows indicate the direction of the current flow [52].	21
3.9	Zeeman splitting of magnetic trapped ^{40}K and ^{87}Rb	22
3.10	Schematic illustration of the magnetic coil configuration for the transport.	23
3.11	Simulation of the currents for the different coils to achieve a loss-free magnetic transport [52].	24
3.12	The interaction of the red detuned light field with the atomic dipole moment generates a force that is directed to the intensity gradient [54].	26
3.13	Schematic illustration of the dipole trap setup.	27
3.14	Left: adiabatic rapid passage for the ^{87}Rb hyperfine transition. Right: Adiabatic rapid passage for the ^{40}K magnetic sublevel transition [52].	28

3.15	Spectroscopy of the transition $ F = 1, m_F = 1\rangle$ to $ F = 2, m_F = 2\rangle$ at a magnetic field of 546,10 G.	29
3.16	Schematic design of the laser.	31
3.17	Orientation of the laser ellipse compared to the grating.	31
3.18	Comparison of a potassium spectroscopy signal.	32
4.1	Level diagram of the ^{87}Rb atom for an external magnetic field. . . .	36
4.2	Example for the calculation of the detuning value.	37
4.3	Schematic illustration of the laser system.	38
4.4	Beat signal with fitted voigt profile	39
4.5	Doppler broadened spectroscopy signal. Indicated with red and blue arrows are the offset lock point and the detection laser lock point respectively.	40
4.6	Fluctuations of the frequency to voltage conversion of the offset lock.	42
4.7	Fluctuations of the lock frequency.	42
4.8	Schematic illustration of the adjustment of the blast light, the detection light and the microwave antenna to the atomic ensemble. . . .	43
4.9	Generation process for the 8 GHz microwave.	44
4.10	Shortening of the antenna tube to improve the output properties. . . .	45
5.1	Transition between the hyperfine states of ^{87}Rb	48
5.2	Spectroscopy signals of the $ F = 1, m_F = 1\rangle$ to $ F = 2, m_F = 2\rangle$ transition with different microwave output power.	49
5.3	Removal of ^{87}Rb atoms, prepared in the $ F = 2, m_F = 2\rangle$ state, plotted against the detuning of the AOM frequency of the blast laser. . .	50
5.4	Measurement of the remaining ^{87}Rb atoms for different pulse lengths of the blast light.	51
5.5	Comparison of the linewidth of the microwave transition with the selectivity of the atom removal due to the combined microwave plus laser system.	51
5.6	Reduction of the laser power to increase the selectivity of the atom removal	52
5.7	Reduction of the laser power to increase the selectivity of the atom removal	53
A.1	Circuit diagram of the current controller.	58
A.2	Circuit diagram of the frequency-to-voltage converter.	59

List of Tables

3.1	Overview of the laser frequencies and output power for operating the experiment with ^{87}Rb and ^{40}K	17
4.1	Frequency to voltage conversion of the offset lock.	41
5.1	Comparison of the selectivity of the combined laser and microwave system	53

Danksagung

Hiermit möchte ich mich bei allen bedanken, die zu dem Gelingen dieser Masterarbeit beigetragen haben, und die mich während des letzten Jahres unterstützt, angeleitet, motiviert, abgelenkt, erfreut, betreut, beraten und ermutigt haben.

An erster Stelle möchte ich mich bei Herrn Prof. Dr. Jan Arlt bedanken für die hervorragende Betreuung. Durch die Aufnahme als HiWi in seiner Gruppe hat er schon früh im Studium meine Begeisterung für sein Fachgebiet wecken können, und sich auch nicht durch den bürokratischen Mehraufwand abschrecken lassen, die erste Masterarbeit in Physik an der Universität Hannover intensiv und stets freundlich zu betreuen.

Bei Herrn Prof. Dr. Wolfgang Ertmer möchte ich mich für die Bereitstellung der nun auch erwiesenermaßen exzellenten Rahmenbedingungen am Institut für Quantenoptik bedanken, sowie für die unkomplizierte Übernahme der Korreferats dieser Arbeit.

Mein besonderer Dank geht an meine Betreuer, Oliver Topić, Dr. Carsten Klempt und Thorsten Henninger. Vom ersten Tag an habt ihr mich kompromisslos freundschaftlich in eure Arbeitsgruppe aufgenommen. Die Arbeit mit euch war nicht nur lehrreich, sondern hat auch sehr viel Spaß gemacht. Jeder einzelne von euch war auf seine ganz eigene Art für mich da und ich kann mich glücklich schätzen, gleich drei so großartige Betreuer gehabt zu haben.

Weiterhin möchte ich mich bei allen anderen Doktoranden, Diplomanden und Mitarbeitern des Instituts bedanken, die allesamt zu der außergewöhnlich guten und freundschaftlichen Atmosphäre beigetragen haben, die dieses Institut auszeichnet. Meinen Freunden und Studienkollegen gebührt der Dank, mich immer wieder unterstützt und ermutigt zu haben und die Jahre des Studiums zu einer tollen, unvergeßlichen Zeit gemacht zu haben. Vor allem Christoph Affeldt, der das letzte Jahr seine Diplomarbeit mit mir zusammen an diesem Institut gemacht hat, gebührt mein Dank, denn er war trotz schwerer Zeiten immer für mich da, und die Teepausen waren jeden Tag eine Bereicherung.

Zuletzt möchte ich meinen Eltern danken, denn sie haben mir alles ermöglicht.

Danke!

Selbstständigkeitserklärung

Hiermit versichere ich, dass ich die vorliegende Arbeit selbstständig verfasst und keine anderen als die angegebenen Quellen und Hilfsmittel benutzt habe.

Hannover, April 4, 2008

(Lisa Kattner)